Gene 830 (2022) 146513

Contents lists available at ScienceDirect

Gene

journal homepage: www.elsevier.com/locate/gene

Lysosomal storage disease associated with a *CNP* sequence variant in Dalmatian dogs

Garrett Bullock [a], Gary S. Johnson [a], Tendai Mhlanga-Mutangadura [a], Scott C. Petesch [b], Samantha Thompson [c], Sandra Goebbels [d], Martin L. Katz [e,*]

[a] Department of Veterinary Pathobiology, College of Veterinary Medicine, University of Missouri, Columbia, MO, USA
[b] University of Pennsylvania School of Veterinary Medicine, Philadelphia, PA, USA
[c] Pocono Peak Veterinary Center, Stroudsburg, PA, USA
[d] Max Planck Institute of Experimental Medicine, Department of Neurogenetics, Hermann-Rein-Str. 3, 37075 Göttingen, Germany
[e] Neurodegenerative Diseases Research Laboratory, University of Missouri School of Medicine, Columbia, MO, USA

A B S T R A C T

A progressive neurological disorder was identified in purebred Dalmatian dogs. The disease is characterized by anxiety, pacing and circling, hypersensitivity, cognitive decline, sleep disturbance, loss of coordination, loss of control over urination and defecation, and visual impairment. Neurological signs first became apparent when the dogs were approximately 18 months of age and progressed slowly. Two affected littermates were euthanized at approximately 7 years, 5 months and 8 years, 2 months of age due to the severity of neurological impairment. The mother of the affected dogs and four other relatives exhibited milder, later-onset neurological signs. Pronounced accumulations of autofluorescent intracellular inclusions were found in cerebral cortex, cerebellum, optic nerve, and cardiac muscle of the affected dogs. These inclusions co-localized with immunolabeling of the lysosomal marker protein LAMP2 and bound antibodies to mitochondrial ATPase subunit c, indicating that the dogs suffered from a lysosomal storage disease with similarities to the neuronal ceroid lipofuscinoses. Ultrastructural analysis indicated that the storage bodies were surrounded by a single-layer membrane, but the storage granules were distinct from those reported for other lysosomal storage diseases. Whole genome sequences, generated with DNA from the two euthanized Dalmatians, both contained a rare, homozygous single-base deletion and reading-frame shift in *CNP* which encodes the enzyme CNPase (EC 3.1.4.37). The late-onset disease was exhibited by five of seven related Dalmatians that were heterozygous for the deletion allele and over 8 years of age, whereas none of 16 age-matched reference-allele homozygotes developed neurologic signs. No CNPase antigen could be detected with immunohistochemical labeling in tissues from the dogs with the earlier-onset disorder. Similar to the later-onset Dalmatians, autofluorescent storage granules were apparent in brain and cardiac tissue from transgenic mice that were nullizygous for *Cnp*. Based on the clinical signs, the histopathological, immunohistochemical, ultrastructural, and molecular-genetic findings, and the finding that nullizygous *Cnp* mice accumulate autofluorescent storage granules, we propose that the earlier-onset Dalmatian disorder is a novel lysosomal storage disease that results from a loss-of-function mutation in *CNP* and that shares features characteristic of the neuronal ceroid lipofuscinoses. That the later-onset disorder occurred only in dogs heterozygous for the *CNP* deletion variant suggests that this disorder is a result of the variant allele's presence.

1. Introduction

The lysosomal accumulation of incompletely catabolized macromolecules is the defining characteristic of a group of heritable disorders known as lysosomal storage diseases (LSDs) (Platt et al., 2018). All of the known LSDs are characterized by Mendelian or single-gene inheritance patterns. Most are inherited as autosomal recessive traits. Among the exceptions, mutations in *IDS* have caused X-linked recessive disease (Wilson et al., 1990); and mutations in *GLA* and *LAMP2* have caused X-linked dominant LSDs (Dworzak et al., 1994; Wang et al., 2011). In addition, LSDs caused by mutations in *DNAJC5* have exhibited an autosomal dominant mode of inheritance (Naseri et al., 2021). At least 53 different genes are well recognized as having harbored sequence variants likely responsible for human LSDs (Platt et al., 2018). Recent reports suggest than *ARSG* and *TBCK* may soon gain recognition as additional causes of human LSDs (Beck-Wodl et al., 2018; Kowalewski et al., 2021). Other genes such as *PPT2*; *ARSK*; *CTSE*; *CTSL*, and *CLCN6* have been reported to cause animal LSDs, but variants in their human orthologs have not yet been identified in LSD patients (Gupta et al., 2003; Poet et al., 2006; Stypmann et al., 2002; Trabszo et al., 2020;

Abbreviations: CNPase, 2′,3′-Cyclic-nucleotide 3′-phosphodiesterase; EM, electron microscopy; IHC, immunohistochemistry; LSD, lysosomal storage disease; CSF, cerebrospinal fluid; GFAP, glial fibrillary acidic protein; Iba1, ionized calcium-binding adapter molecule; WGS, whole genome sequencing; SRA, sequence read archive; NCL, neuronal ceroid lipofuscinosis.

* Corresponding author.
E-mail address: katzm@health.missouri.edu (M.L. Katz).

https://doi.org/10.1016/j.gene.2022.146513
Received 14 January 2022; Received in revised form 31 March 2022; Accepted 14 April 2022
Available online 18 April 2022

Yanagawa et al., 2007). For some of the genes that are currently associated with human LSDs, including *MANBA*, *CTSD*, *CTSF, GRN, ATP13A2* and *ASRG*, LSDs were first identified in laboratory or domestic animals (Abitbol et al., 2010; Ahmed et al., 2010; Awano et al., 2006; Cooper et al., 1988; Farias et al., 2011; Jones and Dawson, 1981; Kowalewski et al., 2012; Tang et al., 2006; Tyynela et al., 2000) and later identified in human patients (Naseri et al., 2021; Kowalewski et al., 2012; Siintola et al., 2006; Smith et al., 2013; Smith et al., 2012; Wenger et al., 1986). Similarly, we here describe a novel LSD of Dalmatian dogs associated with a variant in a gene with a human ortholog that harbors a sequence variant which underlies a leukodystrophy not currently recognized to be an LSD (Al-Abdi et al., 2020).

2. Materials and methods

2.1. Subject dogs

These studies were performed in compliance with the U.S. National Institutes of Health Guide of the Care and Use of Laboratory Animals and were approved by the Institutional Animal Care and Use Committee at the University of Missouri. All samples from dogs were obtained with informed consent from the owners. As sources for DNA, we received 19 EDTA-anticoagulated blood samples and one semen sample from members of a family of purebred Dalmatians which included two littermates that exhibited early-onset neurodegenerative signs and 5 relatives that exhibited late-onset neurodegenerative signs. These disease signs are briefly described in the results section and described in detail in Supplementary file 1. Archived DNA samples from 217 Dalmatians with no known relationships to dogs in the above-described family were also utilized for this study.

2.2. Behavioral observations and clinical evaluations

The owners of the Dalmatian family members and the owners of 30 unrelated Dalmatians over 9 years of age were asked to complete a questionnaire that prompted them to rate their dog's status with respect to 29 behavioral and neurological signs, to indicate the ages at which any abnormalities were first observed, and to provide narratives describing any additional signs they had observed (see Supplementary File 2). In addition, the veterinary records for each of the sampled family members were obtained and reviewed. For dogs deceased at the time this study was initiated; health histories were obtained from the owners.

At approximately 5.5 years of age, the two littermates with early-onset neurological disease underwent examinations by a veterinary neurologist (SCP) that included magnetic resonance (MR) imaging of the brains and standard clinical cerebrospinal fluid (CSF) analysis. For MR imaging, each dog was premedicated with butorphanol (0.2–0.4 mg/kg IV), induced with propofol (1–4 mg/kg IV to effect) and maintained under general anesthesia with sevoflurane inhalant. MR imaging of the head was performed with a 1.5-T scanner (GE LX 1.5 Tesla). Sagittal (T2-weighted), transverse (T2-weighted, FLAIR, T1-weighted, T1-weighted + contrast (Magnevist (gandopentetate dimeglumine, Bayer HealthCare Pharmaceuticals, Wayne, NJ), T2*-gradient echo, diffusion-weighted imaging, apparent diffusion coefficient), and dorsal (T1-weighted, T1-weighted + contrast) plane images were obtained for review. CSF was collected via puncture of the cerebellomedullary cistern in both dogs.

2.3. Dog necropsy and tissue acquisition

Due to the severity of the neurological impairments, the owners of the littermates with the early-onset disease elected euthanasia which was performed via intravenous infusion of pentobarbital when the female littermate was 7 years, 5 months of age and the male littermate was 8 years, 2 months of age. As quickly as possible after euthanasia, the eyes were enucleated and the central areas of the corneas were removed. One eye was then placed in 2.5% glutaraldehyde fixative (2.5% glutaraldehyde, 0.1 M sodium cacodylate, pH 7.4) and the other eye was placed in "immuno" fixative (3.5% formaldehyde, 0.05% glutaraldehyde, 0.12 M sodium cacodylate, 1 mM $CaCl_2$, pH 7.4). The brain was removed from the skull and slices of the parietal lobe cerebral cortex and cerebellar cortex were placed in either immuno fixative or EM fixative (2.0 % glutaraldehyde, 1.12% formaldehyde, 0.13 M sodium cacodylate, 1 mM $CaCl_2$, pH 7.4). The remainder of the brain was divided in half and one half was placed in 10% buffered formalin (Fisher Scientific, Cat. no SF93-4). The other half was frozen. Slices of the heart ventricular wall were also obtained and placed in either the immuno or EM fixatives. All fixed tissues were incubated at room temperature until being further processed for microscopic evaluations.

2.4. Mouse tissues

Brain and heart were obtained from wildtype C57BL/6J mice and *Cnp1*-null mutant (*Cnp*$^{-/-}$) mice (Lappe-Siefke et al., 2003) euthanized at 7 to 8 months of age. Immediately following euthanasia, the tissues were fixed in 4% buffered formalin. The tissues were stored in fixative until further processing for microscopic examinations was performed.

2.5. Microscopic analyses

The fixed dog tissue samples were prepared for light and electron microscopic examination and for immunohistochemistry. A segment of the optic nerve was dissected from the 2.5% glutaraldehyde-fixed eye. The cornea, iris, lens and vitreous were then removed from this eye, and the remaining eyecup was dissected to separate it into 12 specific regions (Whiting et al., 2020). A piece of the eyecup adjacent to the optic nerve head and a slice of the optic nerve were processed for light and electron microscopy. Slices of the EM-fixed cerebral cortex; cerebellar cortex, and heart ventricle were also processed for light and electron microscopy. This processing included secondary fixation in osmium tetroxide and embedding in epoxy resin (Katz et al., 1982). Sections of the resin-embedded tissues were cut at a thickness of 0.4 μm; mounted on glass slides, and stained with toluidine blue. The tissue blocks were then trimmed and sections were cut at thicknesses of 80 to 90 nm, mounted on copper grids, and stained with lead citrate and uranyl acetate. The sections mounted on glass slides were examined with a Leica DMI 6000B microscope, and the sections mounted on grids were examined with a JEOL 1400 transmission electron microscope.

Slices of the immuno-fixed central retina and optic nerve head, cerebral cortex, cerebellar cortex, and heart ventricle were processed for fluorescence microscopy. Slices of the formalin-fixed cerebral cortex and heart ventricles from *Cnp*$^{-/-}$ and wildtype mice were also processed for fluorescence microscopy using the same protocol. Samples were washed with 0.17 M sodium cacodylate, pH 7.4 and then incubated sequentially in 10% and 20% sucrose in the cacodylate buffer for 1 to 2 h each with continuous gentle agitation. The samples were then incubated for approximately 1 h in a 1:1 mixture of the 20% sucrose and OCT medium (Tissue-Plus, Scigen Scientific, Cat. no. 4583). Following this, the samples were incubated in OCT medium in embedding molds for 45 min and then frozen on a block of dry ice. Sections of the frozen samples were cut at a thickness of 8 μm in a Microm HM525 cryostat and mounted on Superfrost-Plus slides (Fisher Scientific, cat. no. 12–550-15). Coverslips were mounted with 0.17 M sodium cacodylate buffer. The sections were examined for autofluorescence using a Zeiss Axiophot microscope equipped with a Prior Lumen 200 light source, Zeiss filter set 487705, which consisted of a 400–440 nm bandpass excitation filter, an FT 460 dichromatic beam splitter, and an LP 470 barrier filter to block emission below 470 nm from reaching the measuring device. In addition, a 515-nm barrier filter was also placed in the emission light path. Fluorescence images were acquired using a Zeiss Neofluor 40x objective with a numerical aperture of 0.75 and an Olympus DP72 digital camera.

Slices of the immuno-fixed cerebral cortex, cerebellum, and optic nerve from the dogs were processed for histological and

immunohistochemical labeling. These samples were embedded in paraffin and sections were cut from the tissue blocks at a thickness of 5 μm. The sections were mounted on glass slides and either stained with standard histological stains or immunolabeled with antibodies specific for glial fibrillary acidic protein (GFAP), ionized calcium-binding adapter molecule 1 (Iba1), 2′3′ cyclic nucleotide 3′ phosphodiesterase (CNPase), and mitochondrial ATPase subunit c as described previously (Villani et al., 2019). The primary antibody directed against CNPase was obtained from BioLegend (cat. no. 836403). The primary antibody directed against GFAP was obtained from Agilent (cat. no. Z033429-2). The primary antibody directed against Iba-1 was obtained from Wako (cat. no. 019–19741). The primary antibody directed against ATPase subunit c was obtained from Abcam (cat. no. ab180149). Immunostaining was performed as described previously (Morgan et al., 2013). The stained sections were examined using a Zeiss Axiophot microscope, and images of the sections were acquired with the Olympus DP72 digital camera.

2.6. Molecular genetic analyses

Genomic DNA was isolated from the canine blood and semen samples as described previously (Katz et al., 2005). The DNA samples from the littermates with the early-onset neurodegenerative signs were submitted to the University of Missouri Genomics Technology Core Facility for genomic library preparation and 2 X 150 bp paired-end whole genome sequencing (WGS) on the Illumina NovaSeq 6000 platform. The targeted sequence coverage was 30x. Sequence reads were mapped to a current canine reference genome assembly (Dog10K_Boxer_Tasha) and aligned with Burrows-Wheeler Aligner (BWA). The resulting SAM files were converted to BAM files and sorted with SAMtools (ver. 1.11). PCR duplicates were then marked with Picard tools (ver. 2.23.8). A modified Genome Analysis Tool Kit (GATK version 3.8) best practices pipeline was used to generate Genome Variant Call Format files (gVCF) for both samples. To help identify rare variants in the Dalmatian sequence in DNA from dogs with the earlier-onset disorder, an additional 2,532 canine whole genome sequences were obtained from the Sequence Read Archive (SRA) (https://trace.ncbi.nlm.nih.gov/Traces/sra/sra.cgi) and used as controls. The SRA BioSample identifiers for all 2,534 whole genome sequences used in this analysis are listed in Supplementary File 3. Variants in each of the control samples were called individually with GATK HaplotypeCaller in gVCF mode, and all sample gVCF files were joined with GATK CombineGVCFs to create a cohort of single-sample files. The samples were jointly genotyped using GATK GenotypeGVCFs, and functional effects of the called variants were predicted with SnpEff software together with Ensembl annotation (Dog10K_Boxer_Tasha, GCA_000002285.4). SnpSift software was used to extract annotated variants from the two Dalmatians, and variant reports were generated by tabulating the annotated output on a Microsoft Excel spreadsheet with GATK VariantsToTable.

Sanger sequencing of a PCR amplicon was used to confirm the presence of a potentially causal single-base deletion (9:20350240delC) detected in the homozygous state in whole genome sequences from the littermates with the earlier-onset disorder. Amplification reactions were conducted in 25 μL volumes with a GoTaq Flexi DNA Polymerase Kit (Promega) and included an initial denaturation at 95 °C for 2 min, followed by 40 cycles of denaturation at 95 °C for 15 s, primer annealing at 60 °C for 30 s, extension at 72 °C for 30 s, and a final extension at 72 °C for 2 min. The PCR primer sequences for this assay were *5′-CTGACAGCGGTGAGAACACT-3′* and *5′-GACCTCCTGGAGATTGTGCG-3′*. Presequencing purification of the resulting amplicons was accomplished with a QIAquick PCR Purification Kit (QIAGEN). Purified amplifications were then submitted to Sequetech Corporation (Mountain View, California) for bidirectional Sanger sequencing.

An allelic discrimination assay was used to genotype DNA samples from individual Dalmatians at 9: 20350240. For this assay, the PCR primer sequences were *5′-TGTCGGGCCTCAGTTTCC-3′* and *5′-CCCTGCGGCCCTTCTG-3′*. The competing probes were *5′-VIC-AGCACCGGCTTCT-NFQ-3′* (reference allele) and *5′-FAM-AGCACCAGCTTCT-NFQ-3′* (mutant allele). The 25 μL reaction mixtures which consisted of the DNA sample, (36 μM) primers, and (8 μM) probes in TaqMan Universal PCR Master Mix (ThermoFisher), were monitored in real time in a StepOnePlus Real-Time PCR System (Applied Biosystems).

2.7. Statistical analysis

The Fisher exact test was performed to test the hypothesis that the incidence of the late-onset neurological signs was higher in the dogs heterozygous for the disease allele than in dogs homozygous for the reference allele.

3. Results

3.1. Behavioral observations and clinical evaluations

All of the dogs evaluated in this study had the physical features characteristic of purebred Dalmatians (Fig. 1) and most were registered with the American Kennel Club. A pedigree showing the relationships among the dogs that were utilized in this study is shown in Fig. 2. Abnormal behavioral signs first became apparent in two littermates, female dog A and male dog B, at approximately 18 months of age and included slowly progressing abnormal behavior, cognitive decline, loss of coordination and apparent visual impairment. See Supplementary File 1 for details. In addition, beginning at approximately 7 years and 6 months of age, dogs A and B had difficulty with balance and would frequently lean against objects or walls for support, tip over while walking, walk into obstacles and often appeared disoriented (see Supplementary videos 1 and 2; note that viewers may find the behaviors shown to be disturbing). Dogs C and D, littermates of the affected dogs, had not exhibited any behavioral or neurological abnormalities when they were last evaluated at the age of 8.5 years. At the same age, however, another littermate (dog E) began exhibiting aggressiveness toward other dogs and tremors that were not previously apparent. Dog F, the mother of dogs A and B, began exhibiting behavioral signs at approximately 11 years of age. Among these were loss of appetite, weight loss,

Fig. 1. Dog B at approximately one year of age.

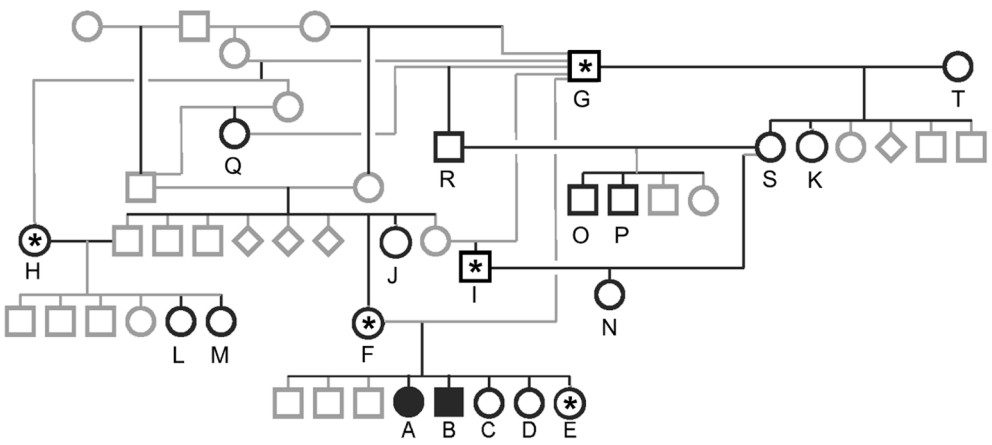

Fig. 2. Pedigree showing relationships among dogs that were evaluated for this study. Symbols above letters represent dogs from which DNA samples and health status information were obtained. Gray-outline symbols represent related dogs whose existence was determined from registration records but from which DNA samples and health information were not obtained. Solid black symbols represent dogs that developed the early-onset disease. Asterisks in symbols indicate dogs that exhibited the late-onset disease. Circle symbols represent females, square symbols represent males. The sexes of the dogs represented by diamond symbols were not provided to us.

restlessness, a moderate loss of housetraining, kyphosis, ataxia, and sleep disturbance. At 12.5 years of age, she would frequently fall and have difficulty standing back up (see Supplementary video 3; viewers may find the behavior shown to be disturbing). Due to the severity of these signs, dog F was euthanized at the age of 13 years, 5 months. Similar neurodegenerative signs were exhibited by the father (dog G) and two other relatives (dogs H and I) starting between 9 and 10 years of age. The clinical details are provided in Supplementary File 1.

Dogs A and B were examined at 5 years of age by a veterinary neurologist (SCP). Detailed results of the examinations are summarized in Supplementary File 1 and Supplementary Video 2. MR imaging of both dogs revealed that marked diffuse cerebrocortical atrophy characterized by enlargement of the lateral and third ventricles, widening of the cerebral sulci, and atrophy of the interthalamic adhesion was present in both dogs (Fig. 3). Both dogs exhibited profound white matter atrophy with periventricular T2w hyperintensity within the caudal internal capsule, and markedly atrophied corpi callosum. Brainstem and cerebellar atrophy were also apparent. No abnormal contrast enhancement was appreciated. A degenerative encephalopathy was prioritized based on the imaging, but a metabolic etiology was not excluded. The only CSF abnormalities were mild albuminocytologic dissociation (CSF protein 38 mg/dL in dog A and 36 mg/dL in dog B, ref. < 30 mg/dL).

3.2. *Microscopic findings in canine tissues*

Fluorescence microscopic examination of unstained cryostat sections of the cerebellar cortex, cerebral cortex, optic nerve, and cardiac muscle, but not the retina, from affected dogs A and B revealed substantial accumulations of autofluorescent material (Figs. 4 and 5). This storage material produced a yellow emission when excited with blue light (400–440 nm). In the cerebellar cortex, the storage material was present primarily in the Purkinje and granule cell layers. In the Purkinje cell layer, only small granules of autofluorescent material were present within the Purkinje cells, whereas large clumps of this material were present in other unidentified cells in this layer (Fig. 4A). In the granule cell layer, the storage material was present primarily as large clusters (Fig. 4B). The autofluorescent material was present, primarily as clumps of granules, in neurons throughout the cerebral cortex (Fig. 4C). The optic nerve contained an abundance of autofluorescent storage bodies that consisted exclusively of small scattered granules (Fig. 4D). Granular

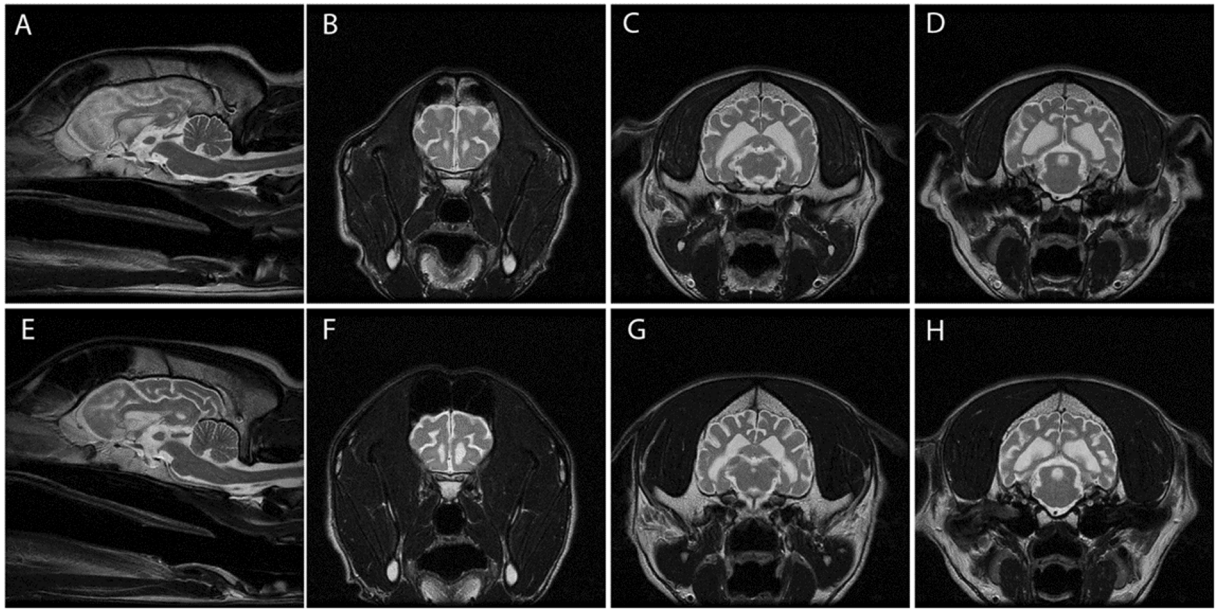

Fig. 3. T2-W MR images of the brains of the two littermates affected with early onset disease at 5 years of age (A to D dog A, and E to H, dog B). Mid-sagittal (A, E) and transverse images at the level of the frontal lobes (B, F), metathalamus and hippocampus (C, G), and caudal colliculi (D, H) showed marked cerebrocortical atrophy with enlargement of cerebral sulci, lateral and third ventricles, and moderate effacement of the interthalamic adhesions. Brainstem and cerebellar sizes appeared normal in the mid-sagittal view.

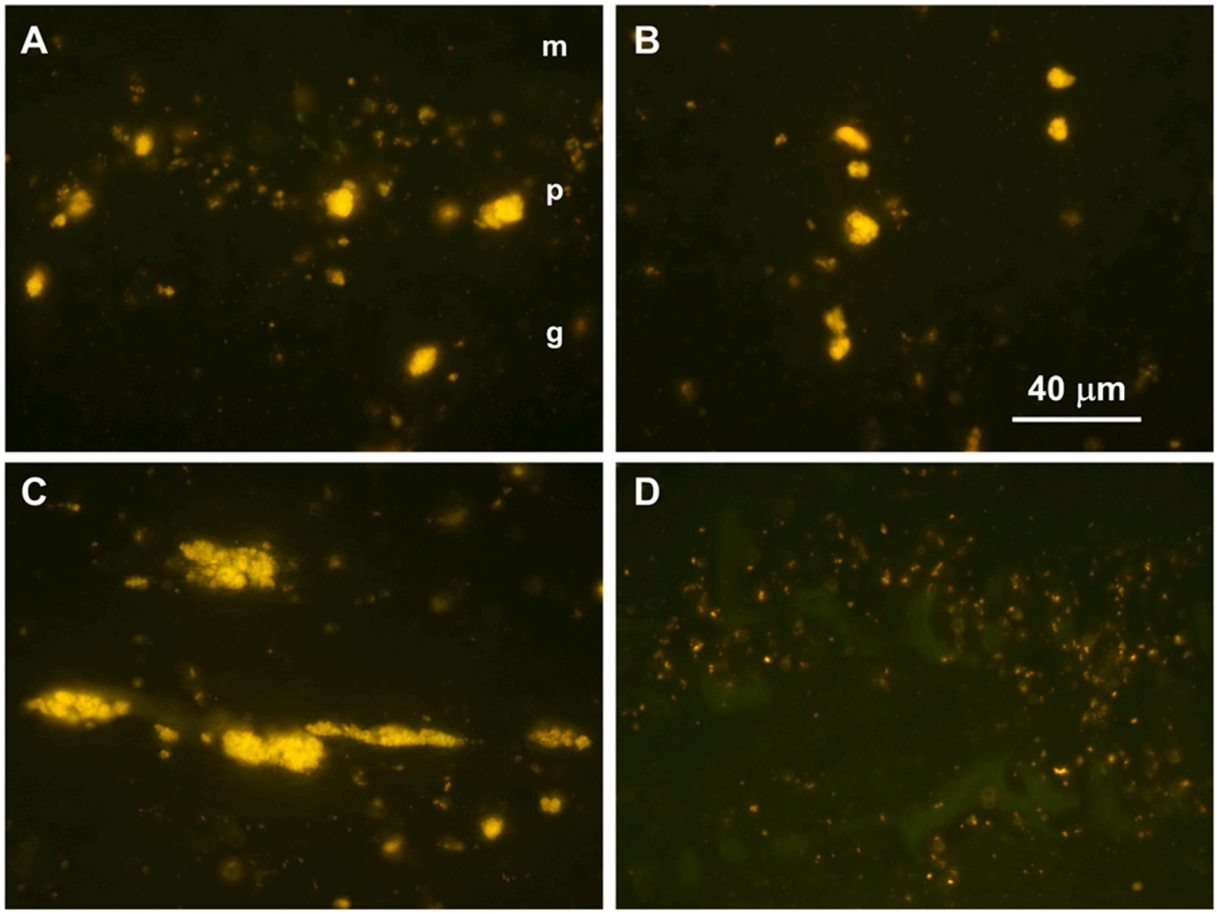

Fig. 4. Fluorescence micrographs of cryostat sections of the cerebellar cortex (A and B), cerebral cortex (C), and optic nerve (D) from dog A showing the yellow-emitting autofluorescent storage bodies in each tissue. Storage bodies were present in cells in the Purkinje (p) and granule cell (g) layers of the cerebellar cortex, but not in the molecular layer (m) (A). The storage material in the cerebellar cortex was most abundant in the granule cell layer (B). Cells throughout the cerebral cortex contained large accumulations of autofluresecent storage material (C). The storage material in the optic nerve (D) consisted of small scattered inclusions rather than the larger clumps seen in the brain. Bar in (B) indicates the magnification of all 4 micrographs. (For interpretation of the references to color in this figure legend, the reader is referred to the web version of this article.)

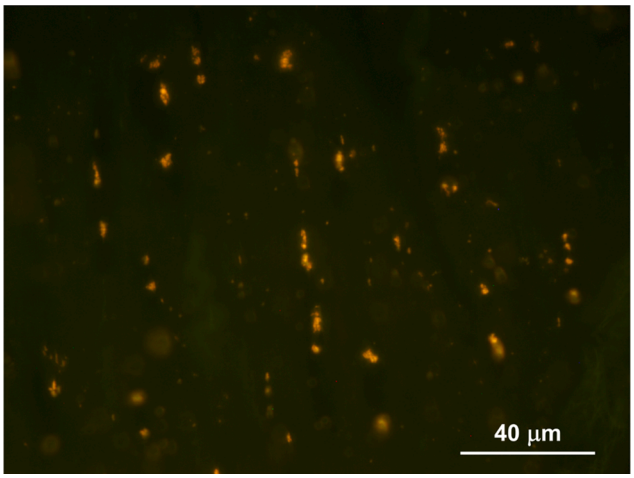

Fig. 5. Fluorescence micrograph of a cryostat section of the heart ventricle wall from the affected dog A showing the yellow-emitting autofluorescent storage bodies in this tissue. (For interpretation of the references to color in this figure legend, the reader is referred to the web version of this article.)

autofluorescent storage material was also abundant in the muscle fibers of the heart ventricular walls (Fig. 5). Most of these storage granules were arranged in strings within cardiomyocytes along the length of the muscle fibers, but some clumps of autofluorescent bodies were present in cells between the muscle fibers.

Electron microscopic examination showed that the cerebellar cortex of dogs A and B contained membrane-bounded intracellular storage bodies with variable ultrastructural appearances. Some of the storage bodies contained clusters of thick-walled vesicular structures of various shapes and lipid droplets (Fig. 6A). Other storage bodies contained fine granular material with embedded spherical lipid droplets of various sizes (Fig. 6B). Although storage bodies with a combination of these ultrastructural appearances were present in many cells, for the most part, individual cells contained predominantly one of these two types of storage bodies. In the cerebral cortex, the ultrastructure of the storage bodies was also variable but differed somewhat in appearance from the storage bodies in the cerebellum. In the cerebral cortex, the contents of some storage bodies consisted of numerous lipid droplets of various sizes interspersed with small vesicular structures (Fig. 7A). The contents of the other storage bodies consisted of a fine granular substance with embedded lipid droplets, primarily at the periphery of the storage bodies (Fig. 7B). Small vesicles were also present within these storage bodies. As in the cerebellum, storage bodies that were intermediate in appearance between these extremes were also observed in the cerebral cortex.

Ultrastructural examination of the optic nerve inclusion bodies in

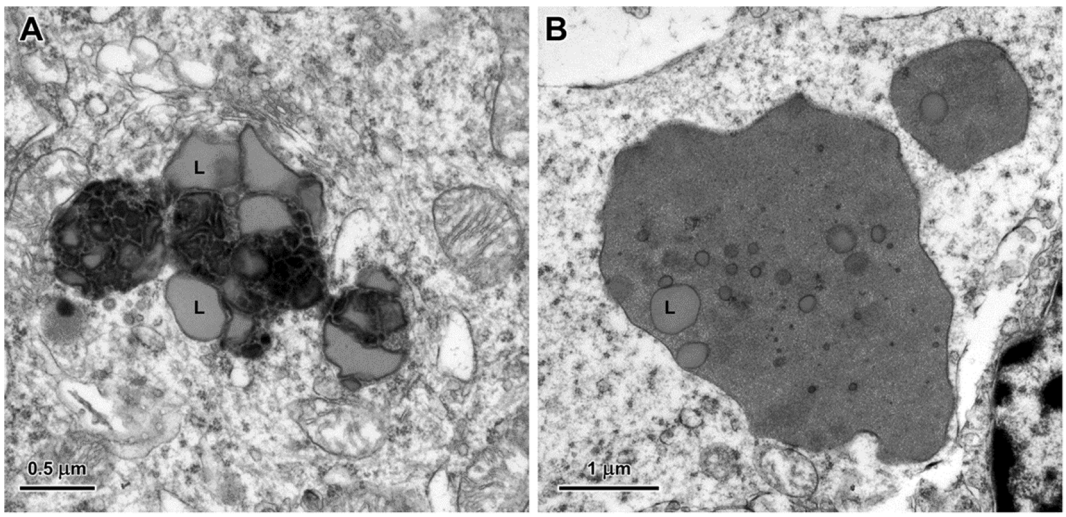

Fig. 6. Electron micrographs showing storage bodies in cells of the cerebellar cortex from dog A. The contents of some storage bodies (A) consisted of clusters of thick-walled vesicular structures interspersed with lipid droplets (L). Other storage bodies (B) contained primarily fine granular material in which lipid droplets of varying sizes are embedded.

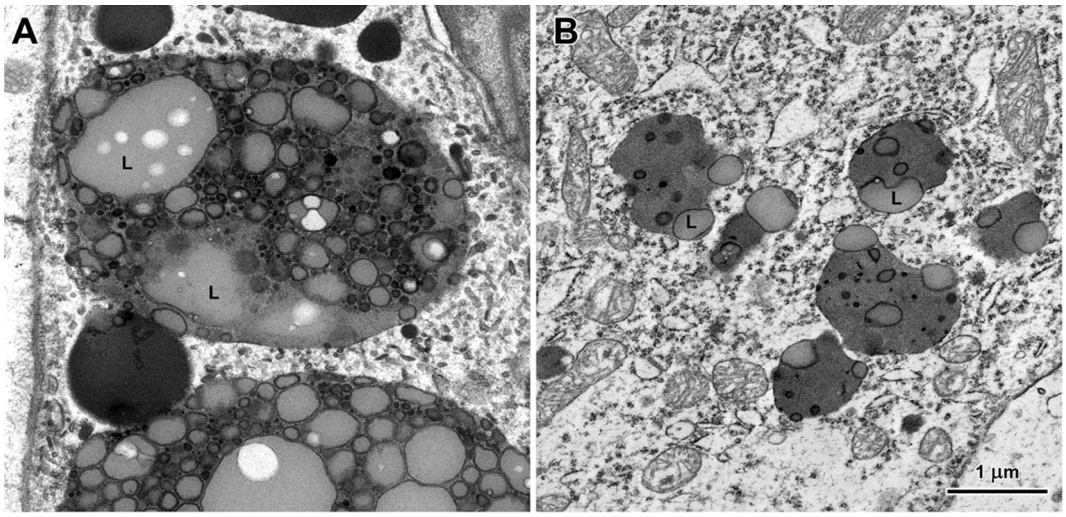

Fig. 7. Electron micrographs showing storage bodies in cells of the cerebral cortex from dog A. The contents of some storage bodies (A) consisted of clusters of small vesicles interspersed with lipid droplets (L). Other storage bodies (B) contained primarily fine granular material in which small vesicles and lipid droplets of varying sizes were embedded. Bar in (B) indicates the magnification of both micrographs.

dog A showed them to contain heterogenous aggregates of distinct components (Fig. 8). These included densely-stained flocculant material, structures with uniform moderate electron density characteristic of lipid droplets, and whorls of membrane-like structures. Most of the myelin sheaths surrounding the optic nerve axons had areas of abnormal splitting between the myelin layers that in many cases appeared to compress the axonal processes (Fig. 9A). Some axonal processes were completely obliterated by disorganized layers of myelin (Fig. 9B).

Light microscopic examination showed that the collagenous extrafascicular matrix that normally divides the optic nerve into distinct fascicles (Whiting et al., 2014; Evans and Jeffery, 1992) was significantly attenuated in dogs A and B such that individual fascicles were no longer separated from one another (Figs. 10 and 11). This attenuation was more pronounced in the dog that was euthanized at 8.2 years of age than in the dog euthanized at 7.4 years of age. There were also numerous areas devoid of myelin-ensheathed axons in both dogs (Fig. 10A), and overall axonal density was lower than normal for dogs (Whiting et al., 2014).

Electron microscopic evaluation of the cardiac ventricular wall muscle revealed two distinct types of inclusion bodies. The inclusion bodies within the cardiomyocytes contained clusters of irregularly-shaped structures consisting primarily of parallel arrays of double-membrane entities (Fig. 12). The second type of inclusions was found in scattered cells located between cardiac muscle fibers. These inclusions were similar in appearance to those found in the brain (Fig. 13).

To determine if the autofluorescence was localized to lysosomes, sections of cerebral cortex and cerebellum from the dog A were immunostained with an antibody that specifically labels the lysosomal marker protein LAMP2. The sections were then examined with fluorescence microscopy to localize the autofluorescent inclusions and with transmitted light to localize the LAMP2 immunostaining. The colocalization of the autofluorescent inclusions and the LAMP2 immunostaining indicated that the autofluorescence originated in lysosome-related inclusions (Fig. 14).

In many forms of NCL, a significant component of the lysosomal storage bodies is the subunit c of mitochondrial ATP synthase (Rowan and Lake, 1995; Katz et al., 1995; Hosain et al., 1995; Vesa and Peltonen, 2002; Cao et al., 2011). Immunohistochemical labeling of cerebral

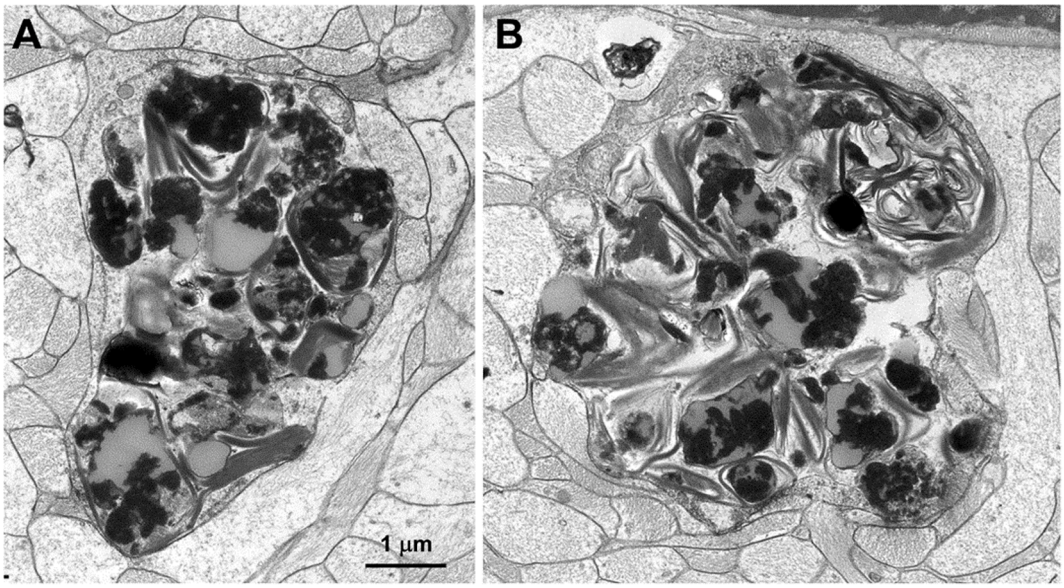

Fig. 8. Electron micrographs of disease-specific cellular inclusions in cells of the optic nerve from dog A.

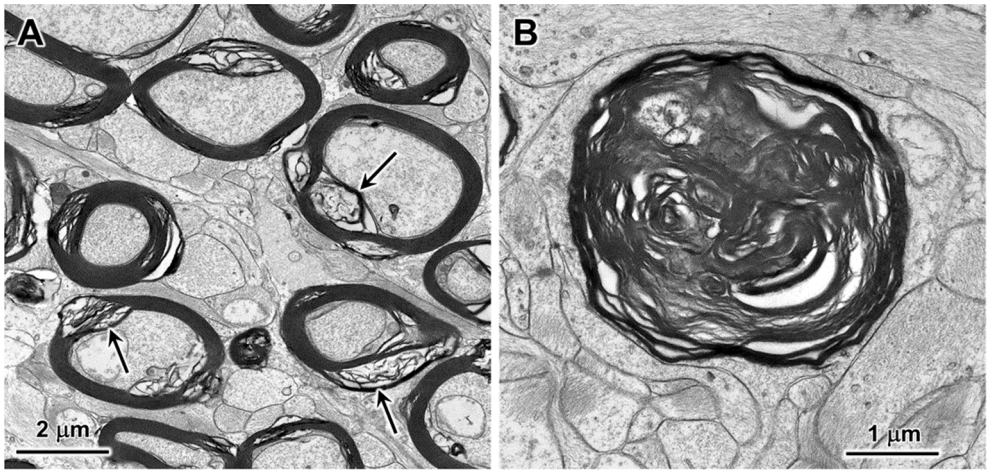

Fig. 9. Electron micrographs showing an almost ubiquitous ballooning of the myelin sheaths surrounding ganglion cell axons in the optic nerve of dog A (arrows in A). Cross sections of scattered axons were almost completed obliterated by abnormally arranged layers of myelin (B).

cortex and cerebellum from the affected dogs demonstrated that the same cells that exhibited autofluorescent storage body accumulation also contained punctate inclusions that were immunopositive for this protein (Fig. 15). This immunolabelling was not detectable in sections of the same tissues from unaffected dogs.

To assess whether the disorder in these dogs was characterized by neuroinflammation, sections of the cerebellum and cerebral cortex from dogs A and B were immunostained with antibodies directed against Iba1 (to detect activated microglia) and GFAP (to detect activated astrocytes). Significant microglial activation was indicated by Iba1 immunolabeling in both brain regions (Fig. 16A and B); however, GFAP immunolabeling did not reveal any significant astrocyte activation in either brain region (Fig. 16C and D).

3.3. Molecular genetic findings

DNA samples from dog A and dog B were used to generate separate whole genome sequences with average coverages of 22.8 and 32.8, respectively. These whole genome sequences were analyzed in conjunction with whole genome-sequence data sets from 2,534 other dogs with no known relationship to dogs A and B. The 5,800,406 called variants that were present in either dog A or dog B, or both, were extracted from all variants in the 2,536 whole-genome-sequence cohort and filtered to identify 45,938 variants that were predicted to alter the primary structure of the encoded gene products. Of these, 10,740 variants had alternate allele frequencies<0.002 in the combined cohort. Only eight of these rare coding variants, in eight different genes, were homozygous in both affected Dalmatians (see Supplementary File 4). Among the eight homozygous variants, a single-base deletion (9:20350240delC) was considered to be the most likely candidate for causality because the deletion occurred in *CNP*, a gene with human and murine orthologs that have previously been associated with progressive neFurodegenerative diseases (Al-Abdi et al., 2020; Lappe-Siefke et al., 2003), and because the deletion resulted in a reading-frame shift predicted to encode a transcript with a premature termination codon {[ENSCAFT00000102206:c.1107del; p.(Lys370AsnfsTer11)}.

The 9:20350240delC allele was absent from all 2,577 control whole genome sequences with called genotypes. The presence of this deletion variant in Dalmatians A and B was confirmed by Sanger sequencing (Fig. 17). We genotyped 237 of our archived DNA samples from

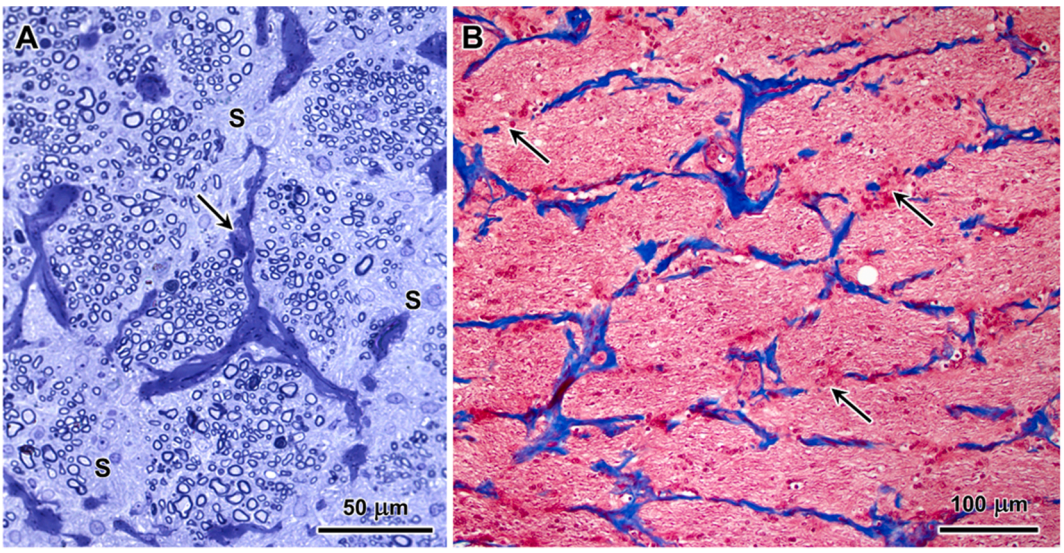

Fig. 10. Light micrographs of optic nerve sections from dog A stained with Toluidine blue (A) and with Masson's trichrome (B). The collagenous extrafascicular matrix that normally separates the optic nerve into fascicles (arrow in A, blue-stained structures in B) was fragmented in dogs A and B, with gaps in the connective tissue strands (arrows in B). There were also large areas devoid of myelin-ensheathed ganglion cell axons (s in A). (For interpretation of the references to color in this figure legend, the reader is referred to the web version of this article.)

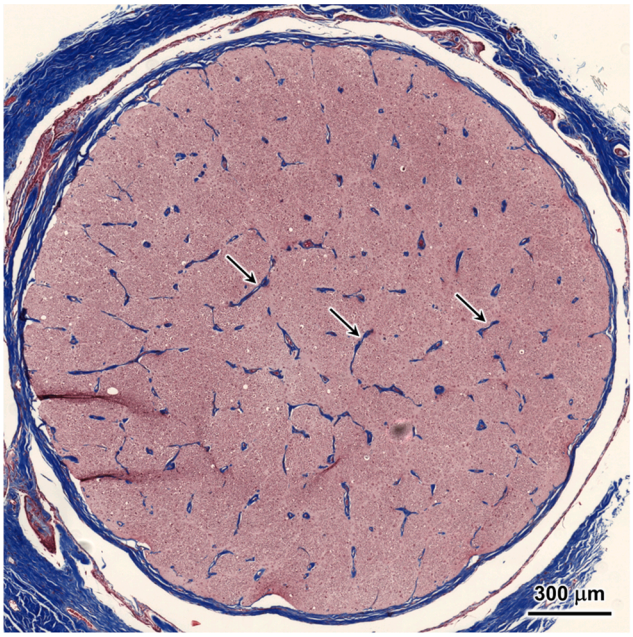

Fig. 11. Light micrograph of optic nerve section from dog B stained with Masson's trichrome showing loss of the collagenous extrafascicular matrix that normally separates the optic nerve into fascicles (blue-stained structures, arrows). (For interpretation of the references to color in this figure legend, the reader is referred to the web version of this article.)

Dalmatians for the 9:20350240delC variant. Only dogs A and B were homozygous for the deletion. All 7 of the dogs that were heterozygous (dogs E to K) are represented in the pedigree in Fig. 2. Five of the heterozygotes (dogs E to I) exhibited late-onset neurodegenerative signs. The other two heterozygotes (dogs J and K) had not been reported to exhibit neurologic abnormalities at the ages at which health status information was last obtained (dog I at 9.5 years and dog J at 11 years). In addition, we obtained clinical information for six 9-years-old or older Dalmatians with no known relationship to the family in Fig. 2. All were homozygous for the reference allele and none had signs of neurologic disease. Thus, among Dalmatians over 8 years old with available clinical records, five of seven that carried the deletion allele in the heterozygous state developed the late-onset disease; whereas, zero of 16 reference-allele homozygotes exhibited signs of late-onset neurologic disease. Based on the Fisher exact test, there was a significant association between the development of the late onset disease and heterozygosity for the deletion allele ($p < 0.001$).

3.4. Microscopic findings in *Cnp*$^{-/-}$ mouse tissues

To determine if *Cnp* deficiency was associated with the accumulation of autofluorescent storage bodies in a genetically engineered mouse model, formalin fixed brain and heart tissues from 7-to-8 month old *Cnp*$^{-/-}$ mice were evaluated for the accumulation of autofluorescent cellular inclusions using the same procedures used to evaluate the dog tissues. Autofluorescent inclusions were abundant throughout the brain and cardiac muscle (Fig. 18), but were not present in the same tissues from age-matched wildtype mice of the same strain (C57BL). As with dogs A and B, the inclusions in the hearts of the *Cnp*$^{-/-}$ mice were present in both the muscle fibers and in cells between the muscle fibers, but they were less abundant than in the cardiac muscle obtained from the affected dogs at disease end stage.

3.5. Cnpase immunohistochemistry

Immunohistochemistry was employed to determine how the homozygous 9:20350240delC genotype affects expression of CNPase antigen. Immunohistochemical labeling of sections of the cerebellum, cerebral cortex, optic nerve, and cardiac muscle from affected dogs A and B with polyclonal anti-CNPase antibodies failed to detect any CNPase protein in these tissues. CNPase immunolabeling of the same nervous tissues from an unaffected Australian Shepherd was pronounced, particularly in nerve fiber tracts (Fig. 19). The cardiac muscle tissue from the latter dog contained scattered cells with strong CNPase immunostaining that were located between the muscle fibers (Fig. 20). No CNPase immunolabel was detected in the cardiac muscles from dogs A and B.

4. Discussion

We obtained DNA samples from 20 closely related Dalmatian dogs,

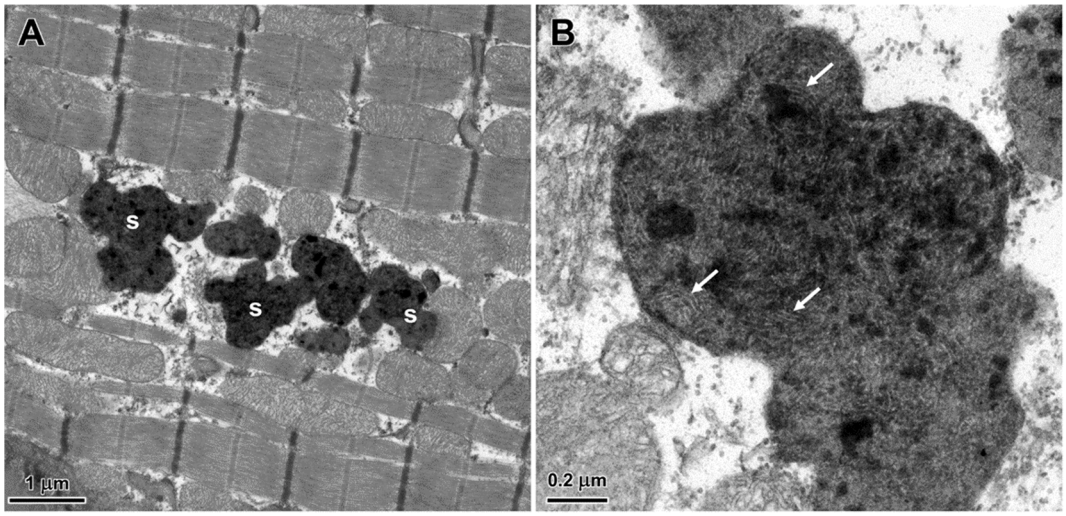

Fig. 12. Inclusion bodies (s) within cardiomyocytes of the dog A (A). At higher magnification, the contents of these inclusions were rich in parallel arrays of double-membrane structures (arrows in B) and scattered clumps of electron-dense amorphous material.

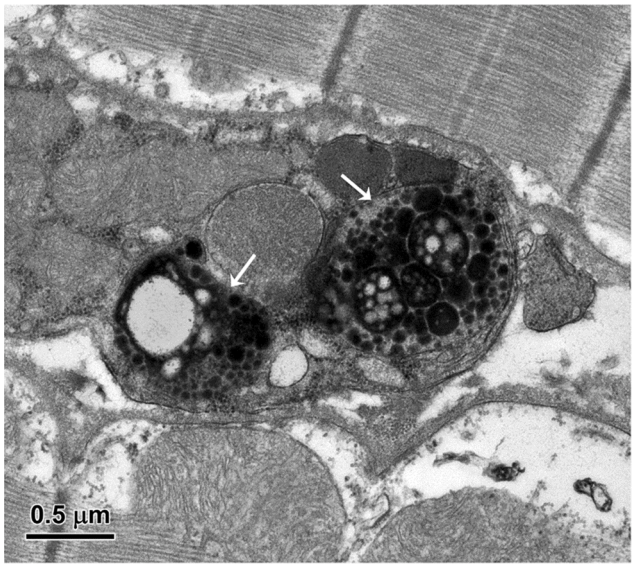

Fig. 13. Inclusion bodies (arrows) in a cell between two adjacent myocytes. Based on their locations and morphology, cells within the heart ventricular muscles that contained inclusions with this type of ultrastructural appearance are most likely telocytes, within which the inclusions were present in the telopodes (Gherghiceanu and Popescu, 2012; Kostin, 2016).

including two littermates that suffered from a severe progressive neurological disorder with an onset of clinical signs at approximately 18 months of age. The severity of the signs progressed slowly over the following six years, when the dogs were euthanized due to the severity of their neurological deficits. MR imaging of these dogs showed marked generalized brain atrophy with pronounced white matter degeneration. Five of the remaining related dogs exhibited progressive neurological signs that were less severe and had much later onsets of 9 to 11 years of age. The dogs exhibiting this later-onset disease phenotype included both of the parents and one littermate of the dogs with the earlier-onset disorder, as well as two other relatives. None of the other 13 dogs in the family exhibited signs of neurological disease. Therefore, investigations were undertaken to characterize the disease phenotypes, identify the molecular genetic causes and determine if the early- and late-onset disorders had a common genetic cause.

Brain, optic nerve, retina and heart tissues obtained from the dogs with the earlier-onset disorder were examined to characterize the disease pathology. Among the pathological signs in all tissues examined except the retina were accumulations of intracellular autofluorescent inclusion bodies. The inclusion bodies were each bounded by a single biomembrane and contained material with complex, heterogeneous ultrastructural appearances that varied within and between tissue types. Many of the storage bodies appeared to contain lipid droplets and vesicles. In cardiac muscle, the autofluorescense was detected both within and between the muscle fibers. Three cell types are present between the muscle fibers: Schwann cells, fibroblasts, and telocytes which have long extensions (telopodes) (Gherghiceanu and Popescu, 2012; Kostin, 2016). Based on this morphological feature, the *CNP*-expressing cells between the muscle fibers are likely to be telocytes. The autofluorescence in the tissues colocalized with immunostaining for the lysosomal marker LAMP2, suggesting that the disorder should be classified as an LSD. The unique ultrastructural appearance of the storage body contents, a concomitant myelin pathology, and the pattern of clinical signs suggested that the disease is distinct from previously recognized lysosomal storage disorders.

Consistent with this suggestion, the whole genome sequences of the two littermates with early-onset disease did not contain likely causal variants in any of the genes previously associated with LSDs. Instead, a rare, homozygous single-base deletion and frameshift near the 3′-end of *CNP*, the gene that encodes CNPase, was found to be the likely cause for the disease. Two subsequent findings added strong support to the view that homozygosity of the *CNP* deletion caused the disease. Autofluorescent storage bodies, similar to those in dogs A and B, were found in formalin-fixed brain and heart tissue from *Cnp*$^{-/-}$ mice. In addition, immunohistochemical analysis with an anti-CNPase antibody strongly stained brain tissue from an unaffected control dog but failed to produce detectable staining with brain tissue from the affected littermates. Although variants in *CNP* orthologs are published causes of human and murine neurodegenerative diseases (Al-Abdi et al., 2020; Lappe-Siefke et al., 2003), these disorders have not previously been reported to be LSDs. In the case of the affected human subjects, tissue samples were not obtained for microscopic examination. Based on our findings, we predict that similar storage material will be found, at least in neural tissues, from future human patients with *CNP* deficiency, should these tissues become available.

Similarities between the disease phenotypes in the Dalmatians with the early-onset disorder and the *Cnp*$^{-/-}$mouse model further support the *CNP* single-base deletion and frameshift as the direct cause of the canine disease. A 2003 report described the creation and characteristics of the

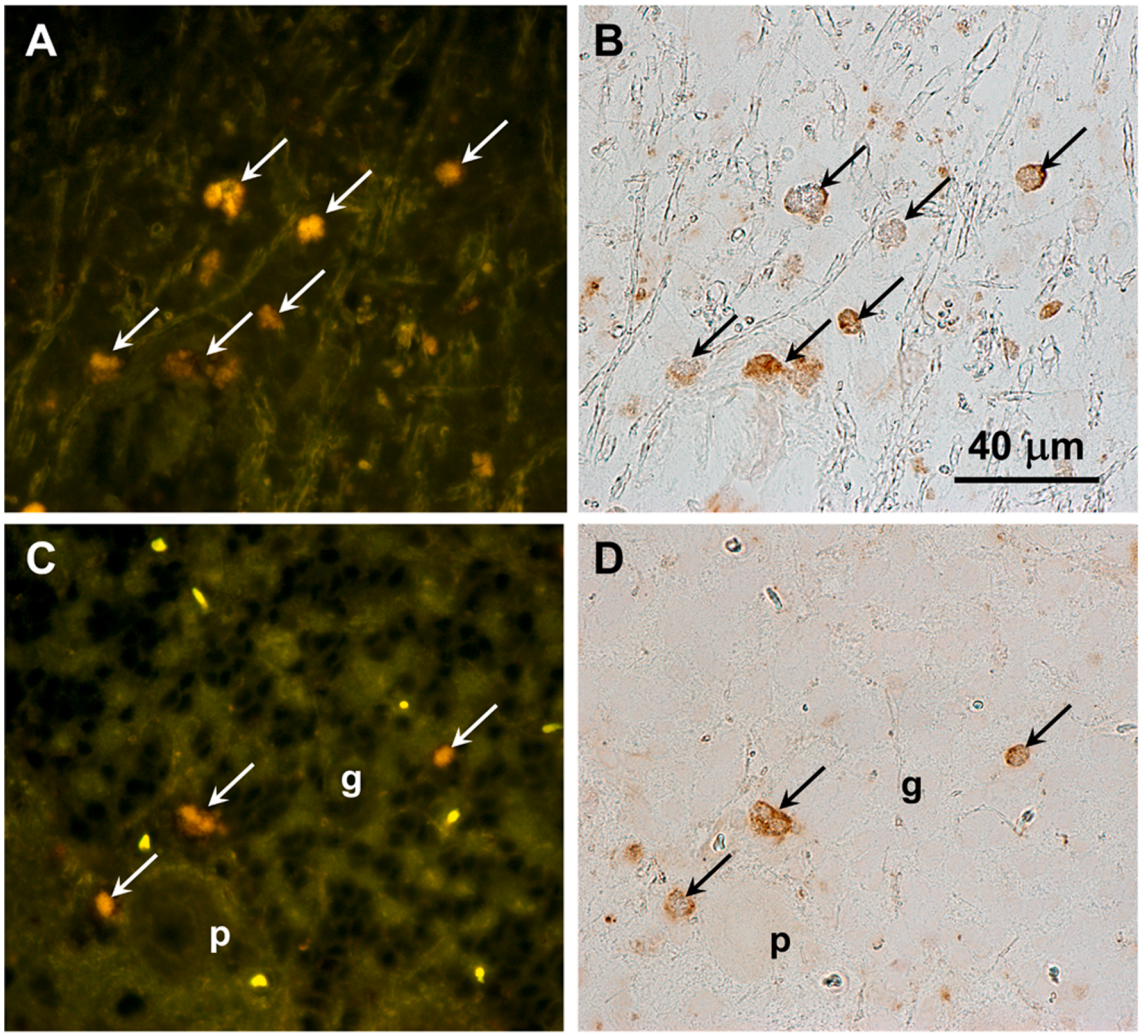

Fig. 14. Sections of parietal cerebral cortex (A and B) and cerebellar cortex (C and D) from dog A immunostained for the lysosomal marker protein LAMP2. Sections were photographed to demonstrate inclusion body autofluorescence (arrows in A and C) and LAMP2 immunostaining (arrows in B and D). The autofluorescence co-localized with the immunostaining. In C and D, p = Purkinje cell; g = granule cell layer. Bar in B indicates magnification of all 4 micrographs.

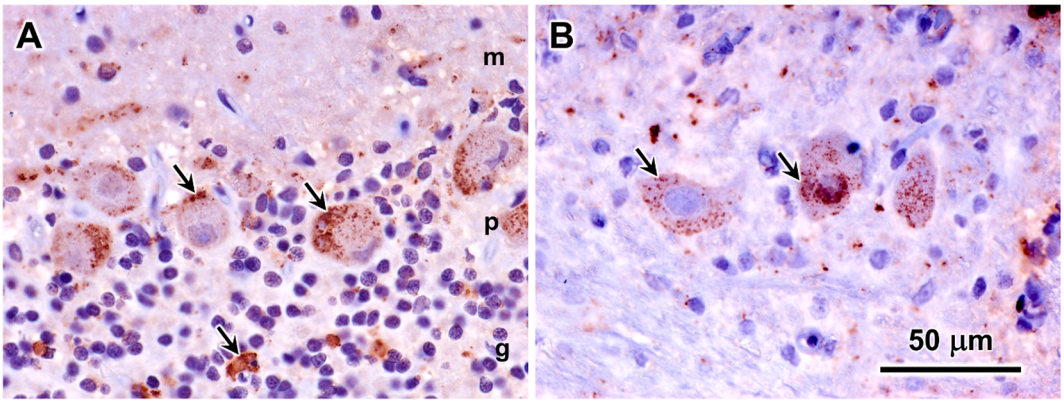

Fig. 15. Sections of the cerebellum (A) and cerebral cortex (B) from dog B immunolabeled with an anti-ATPase subunit c antibody. Punctate immunolabel (brown–red; arrows) was observed in all layers of the cerebellar cortex (m: molecular layer; p: Purkinje cell layer; g: granule cell layer), and in neurons in the cerebral cortex. Bar in (D) indicates magnification of all 4 micrographs. (For interpretation of the references to color in this figure legend, the reader is referred to the web version of this article.)

Cnp$^{-/-}$ mouse model (Lappe-Siefke et al., 2003). The *Cnp*$^{-/-}$ mice appeared to develop normally until they reached adulthood. At 4 months of age; *Cnp*$^{-/-}$ mice exhibited slowly progressive neurogenerative signs that in most cases culminated in premature death before they reached one year of age. Among the disease signs were ataxia, weight loss, hind limb paralysis, convulsions, gait abnormalities, and kyphosis. Post-mortem

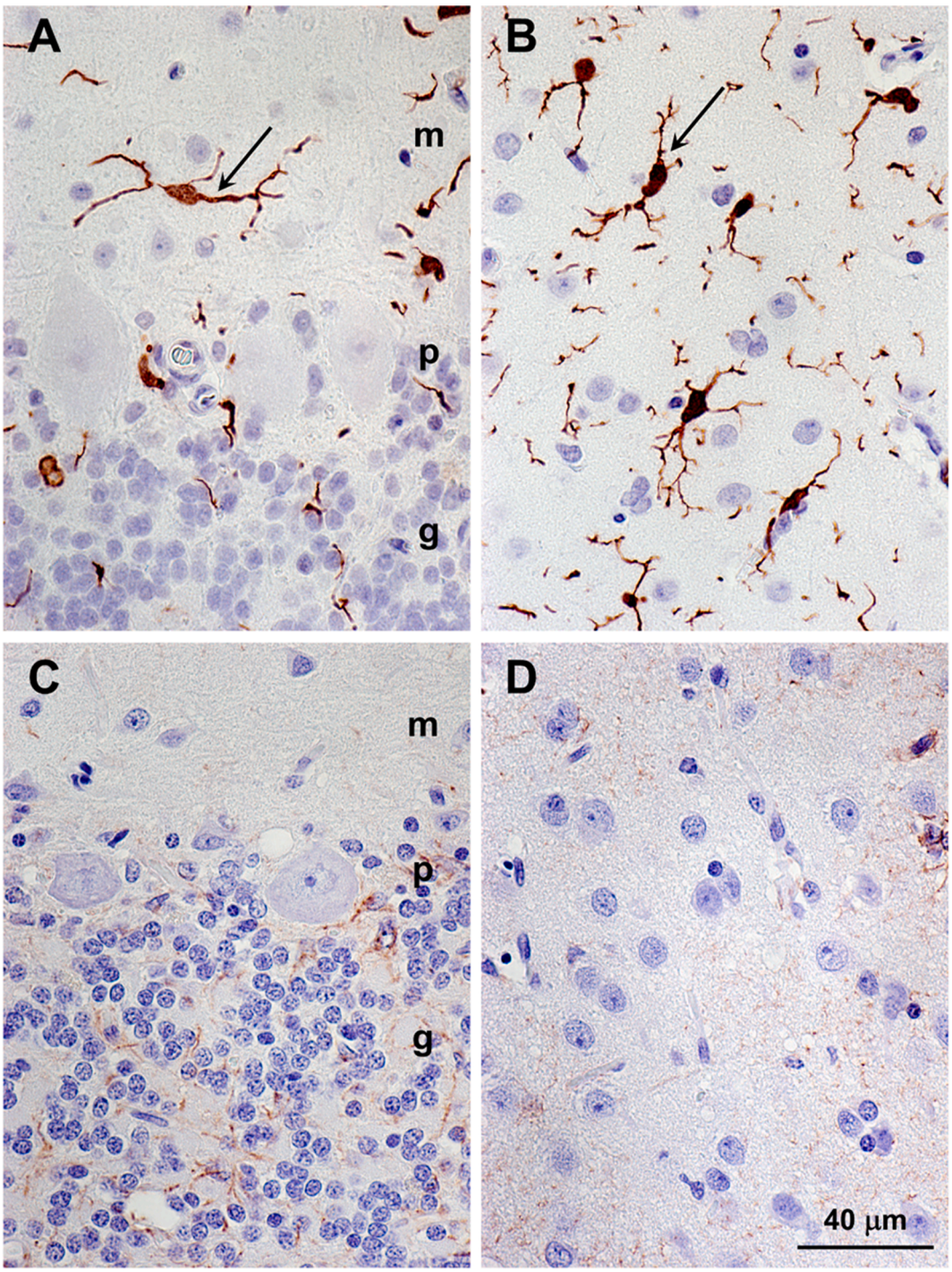

Fig. 16. Sections of the cerebellum (A) and cerebral cortex (B) from dog A immunolabeled with an anti-Iba1 antibody. Labeled cells appear brown (arrows). Sections of the cerebellum (C) and cerebral cortex (D) from dog A immunolabeled with an anti-GFAP antibody. Minimal immunolabeling was observed. Cerebellar layers are m: molecular layer; p: Purkinje cell layer; g: granule cell layer. Bar in (D) indicates magnification of all 4 micrographs.

findings included generalized brain atrophy characterized by ventricular enlargement and white matter loss which became apparent by seven months of age. Abnormal axonal swellings were seen in spinal cord nerve tracts and optic nerves of aged *Cnp*$^{-/-}$ mice. Within these spheroids were membranous organelles and multivesicular bodies with ultrastructural appearances that were similar to the inclusions observed in the neural tissues, including the optic nerve axons, of dogs A and B (Lappe-Siefke et al., 2003). Both the affected dogs and the *Cnp*$^{-/-}$ mice exhibited myelin abnormaltiies that are not typical of other LSDs. Enlarged myelin inner tongues were present in *Cnp*$^{-/-}$ neonates and persisted throughout life (Edgar et al., 2009). These may correspond to the ballooning of the myelin sheathes we observed in the optic nerves from the affected Dalmatians. In addition; the *Cnp*$^{-/-}$ mice exhibited disorganization of the paranodal structures in the optic nerve myelin sheaths after 3 months of age (Rasband et al., 2005). Thus; both lysosomal storage body accumulation and myelin abnormalities are associated with *CNP* deficiency.

A common feature of many progressive neurodegenerative disorders is neuroinflammation. This was observed in both dogs A and B and in the *Cnp*$^{-/-}$ mice (Lappe-Siefke et al., 2003); however, the mice exhibited both

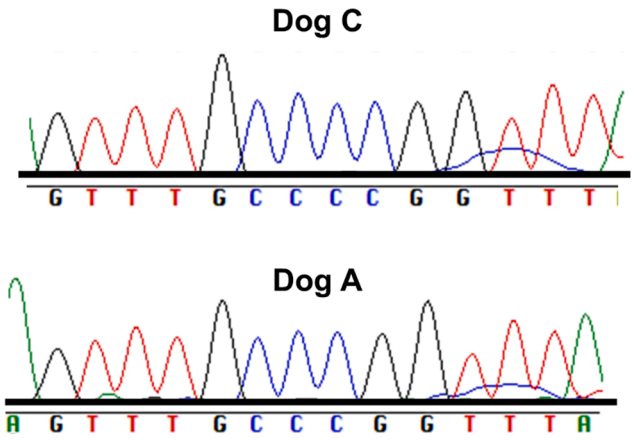

Fig. 17. Sanger sequencing validation of the 9:20350240delC variant in affected dog A compared to unaffected littermate dog C.

astrogliosis and microgliosis whereas the affected Dalmatians had a prominent microgliosis but little or no evidence of an astrogliosis. Overall, the similarities in the disease phenotype of the dogs with the earlier-onset disorder and *Cnp*$^{-/-}$ mice support the conclusion that the Dalmatian disease is due to the *CNP* deletion variant that was exclusively homozygous in the littermates with the earlier-onset disease phenotype.

Five of seven Dalmatians that were at least 9 years old and heterozygous for the single-base deletion and frameshift in *CNP* exhibited the later-onset neurodegenerative disease phenotype. In contrast, none of 16 Dalmatians that were homozygous for the reference allele and were over 9 years of age exhibited this clinical phenotype. Because the late-onset disease was unique to the heterozygous dogs, it is very likely that this disease is the result of heterozygosity for the *CNP* deletion variant. This conclusion is supported by phenotypic characterization of mice that were heterozygous for the *Cnp* knockout allele. A 2012 report described immuno-histopathologic and behavioral differences between 24-month-old mice that were either heterozygous for the *Cnp* knockout allele (*Cnp*$^{+/-}$) or wild-type (*Cnp*$^{+/+}$) (Hagemeyer et al., 2012). Compared to 4-month-old mouse brains, the brains from both groups of aged mice had age-related increased axonal swelling, astrogliosis, microgliosis and decreased CNPase expression. However, these differences were more prominent in the *Cnp*$^{+/-}$ compared to the *Cnp*$^{+/+}$ mice. In addition, compared to the aged *Cnp*$^{+/+}$ mice, the aged *Cnp*$^{+/-}$ mice showed significant abnormal behavioral differences that included catatonic gripping, reduced social interest and increased fear memory. The investigators considered the behavioral changes in the aged *Cnp*$^{+/-}$ mice to be indicative of a catatonia-depression syndrome (Hagemeyer et al., 2012). The fact that both dogs and mice heterozygous for *CNP* disease alleles exhibited late-onset neurological signs supports the hypothesis that the late onset Dalmatian disease is the result of *CNP* haploinsufficiency.

The marker, rs2070106, is a synonymous single-nucleotide polymorphism in the last exon of human *CNP*. Between 2006 and 2018, nine investigations of possible associations between rs2070106 alleles and *CNP* transcript expression, regional changes in brain white matter density, and the risks for schizophrenia and/or catatonia have reached diverse conclusions (Hagemeyer et al., 2012; Peirce et al., 2006; Mitkus et al., 2008; Iwamoto et al., 2008; Tang et al., 2007; Voineskos et al., 2008; Usui et al., 2006; Che et al., 2009; Cannon et al., 2012; Janova et al., 2018). More recently; a report of a human Mendelian disease caused by a *CNP* variant appeared (Al-Abdi et al., 2020). A homozygous S82L *CNP* missense mutation was identified as the likely cause of a novel neurodegenerative disease in three siblings from Oman. Unlike the *CNP*-associated diseases in the Dalmatian siblings and the *Cnp*$^{-/-}$ mice with young-adult onsets and survival past middle age, the affected children exhibited clinical signs before they were two years old and all three died before their 9th birthdays. Among the clinical signs were failure to develop independent walking, hirsutism, cognitive and motor impairment, hypertonia, convulsions, seizures, impaired swallowing ability, constipation, ptosis, spastic quadriparesis, and scoliosis. Magnetic resonance imaging of 2 of the affected children showed brain atrophy with profound white matter loss. Visual deficits were not reported in any of the affected children. Although no postmortem examination of tissues was reported, a fibroblast culture was established from one affected child. Western blots of protein extracted from the cultured fibroblasts detected only traces of CNPase, strongly supporting the causality of the *CNP* variant. In addition, an abnormal increase in actin filament intensity was detected in the cultured fibroblasts, which may be a clue to the pathogenesis. If future cases of human *CNP*-deficiency disease exhibit early onsets and rapid progressions like those reported for the Omani children, it should be possible to evaluate potential species differences in CNPase function.

Because dogs heterozygous for the *CNP* disease variant and *Cnp*$^{+/-}$ mice exhibited late-onset neurological signs, it would be of interest to determine whether late-onset neurologic disease is exhibited by aged heterozygous relatives of the affected Omani children. The neurological phenotypes of heterozygous dogs and mice suggest that heterozygosity for *CNP* variants can cause late-onset disease. The ages of the parents were not provided in the report on the affected children, but based on the ages of these children, the parents were likely to be relatively young when the study was performed. The grandparents were not evaluated (Fowzan S. Alkuraya, personal communication), so it is not currently known whether heterozygosity for the human disease allele is associated with late-onset neuropathology. It may be worthwhile to monitor the parents as they age and to screen human subjects exhibiting late-onset neurological signs for potentially deleterious heterozygous variants in *CNP*.

The mechanisms underlying the neurodegeneration in the Dalmatians are unclear because there is no consensus about the relative importance of a variety functions attributed to the proteins encoded by *CNP*. This gene encodes two 2′-3′-cyclic nucleotide 3′-phosphodiesterase (CNPase; EC 3.1.4.37) isoforms that result from two alternative promoters each with a different transcription start site (Fig. 21A) (Kurihara et al., 1990). The two isoforms are identical except that the larger isoform has an amino-terminal twenty amino acid extension that provides a mitochondrial targeting signal. In the adult, the shorter transcript is highly expressed in myelin-producing oligodendrocytes and Schwann cells; whereas, the longer transcript is expressed by a wide variety of cell types but at lower levels (Lee et al., 2006). Both isoforms have identical C-terminal ends which mediate anchoring of the CNPase to biomembranes (Bifulco et al., 2002; Esposito et al., 2008). Because the single-base deletion and frameshift in the canine *CNP* variant is predicted to encode a transcript lacking the normal codons for the 51 C-terminal amino acids of CNPase (Fig. 21B), even if the variant protein were synthesized, the mutation would likely impair the binding to membranes which may be essential for normal function. Both isoforms can catalyze the hydrolysis of 2′-3′-cyclic nucleotides to 2′-nucleotides in vitro (Braun et al., 1991). The 2′-3′-cyclic nucleotide 3′-phosphodiesterase activity appears to be essential for some but not all of the functions proposed for CNPase. One proposed function for the CNPase enzymatic activity involves the hydrolysis of 2′-3′-cyclic adenosine monophosphate (cAMP) to 2′-AMP that can be further hydrolyzed to adenosine which has neuroprotective properties (Verrier et al., 2013). Most of the CNPase that is targeted to the mitochondria becomes bound to the inner mitochondrial membrane (Lee et al., 2006). There, CNPase may have a protective function by catalyzing the hydrolysis of cAMP and other 2′-3′-cyclic nucleotides which can promote the opening of the permeability pore leading to mitochondrial swelling and apoptosis (Azarashvili et al., 2009; Olga et al., 2020).

Protein-protein interactions rather than cyclic-phosphodiesterase activity may drive other functions suggested for CNPase. A number of

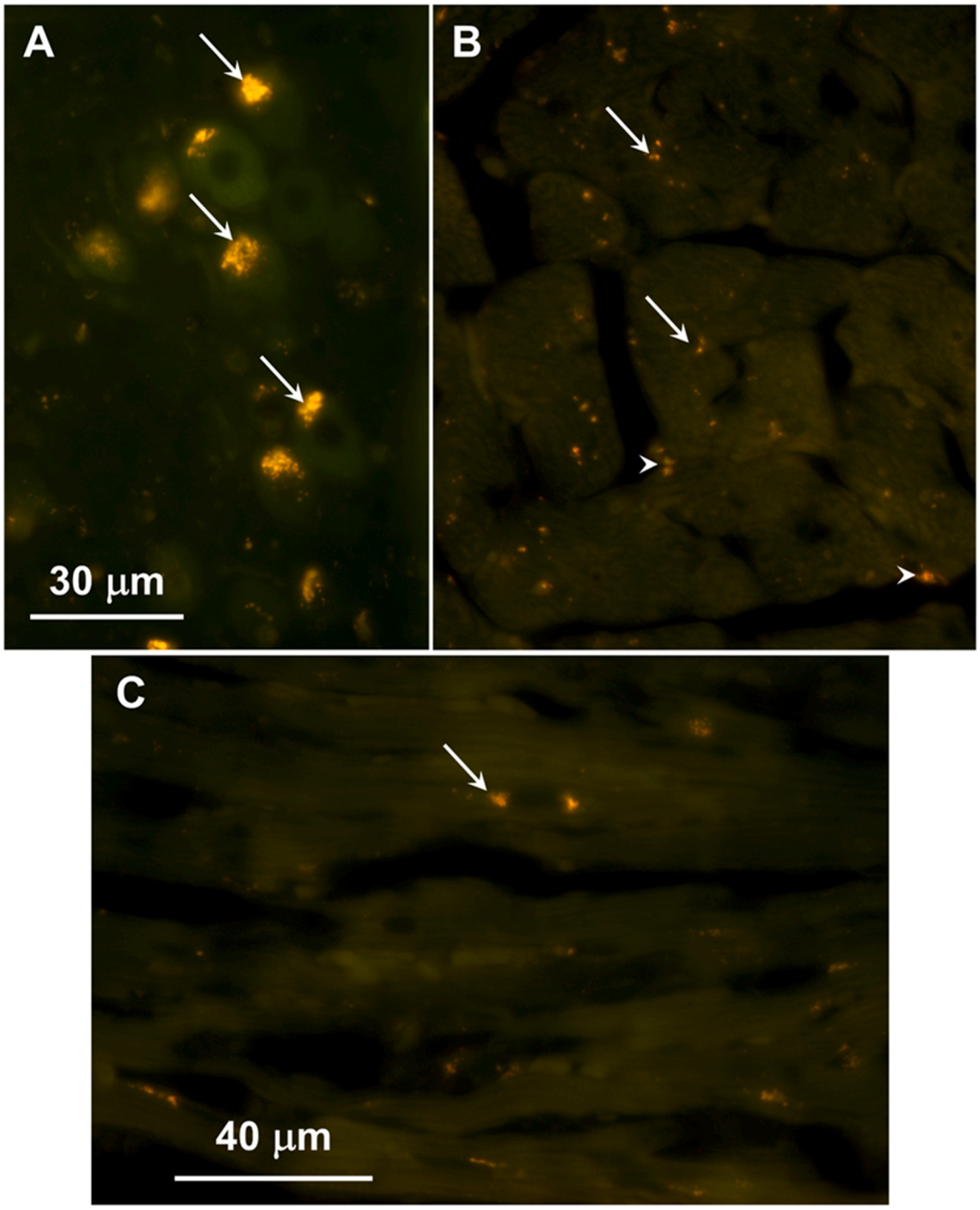

Fig. 18. Fluorescence micrographs of cryostat sections of the cerebral cortex (A) and cardiac muscle (B and C) of a 7-month-old *Cnp*$^{-/-}$ mouse. In (B) the muscle fibers were cut in cross-section and in (C) they were cut in longitudinal orientation. Arrows indicate autofluorescent inclusions within cerebral cortical neurons (A) and cardiac muscle fibers (B and C). Arrowheads indicate inclusions in cells between the cardiac muscle fibers. Bar in (A) indicates magnification for both (A) and (B).

studies indicate that CNPase plays a role in modulating components of the cytoskeleton involved in determining cell shape and mediating intracellular vesicular transport. Early reports indicated that CNPase binds to two major cytoskeletal proteins, tubulin and actin (Laezza et al., 1997; De Angelis and Braun, 1996). CNPase can promote microtubule assembly and reorganization (Bifulco et al., 2002). Interactions between CNPase and cytoskeletal components may be important within myelin sheaths where CNPase appears to function as a structural component required to maintain non-compacted nanochannels that allow the flow of trophic substances from the surrounding glia to the ensheathed axons (Snaidero et al., 2017). Within the cytoplasm of cultured cells, CNPase binds tubulin dimers facilitating microtubule polymerization and reorganization (Lee et al., 2005). In cultured oligodendrocytes and other cells, both CNPase over-expression and CNPase ablation have been shown to alter cell morphology (Lee et al., 2005; Gravel et al., 2009). Thus, the abnormal morphology of the optic nerve axon myelin sheaths in dogs A and B may be secondary to abnormalities in the cytoskeletons of the oligodendrocytes.

It is likely that in addition to cell morphology, CNPase contributes to the regulation of other cytoskeleton-driven processes such as intracellular vesicular trafficking (Anitei and Hoflack, 2011). Therefore, the accumulation of lysosomal storage bodies in the Dalmatian siblings A

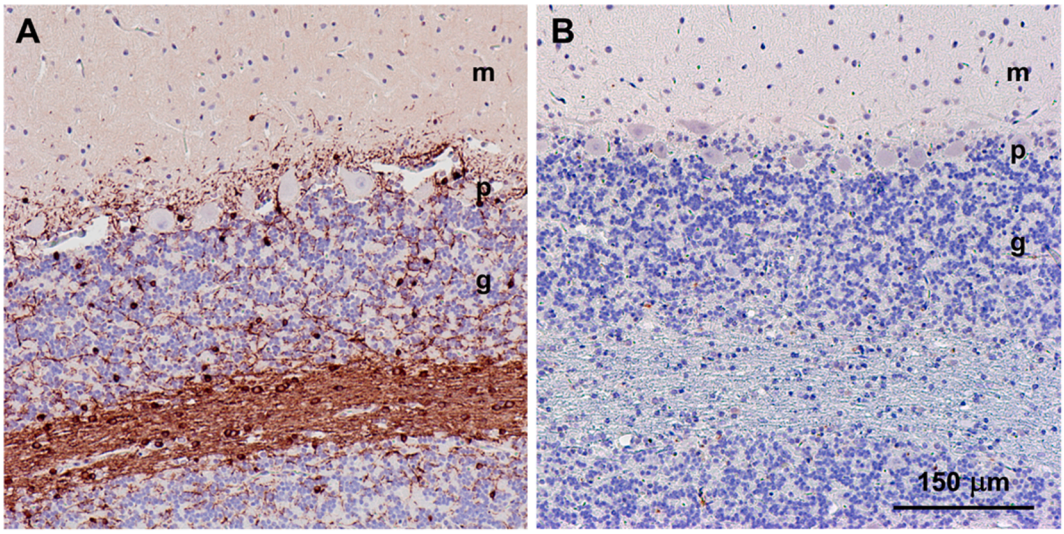

Fig. 19. Sections of the cerebellar cortex from control Australian Shepherd (A) and from dog B (B). Sections were immunostained with an anti-CNPase antibody. Immunolabeling was abundant in the control (brown color in A), particularly in the nerve fiber layer beneath the granule cell layer (g). Almost no immunolabel could be detected in the tissue from dog B. Molecular layers (m), Purkinje cell layers (p), and granule cell layers (g) are labeled.

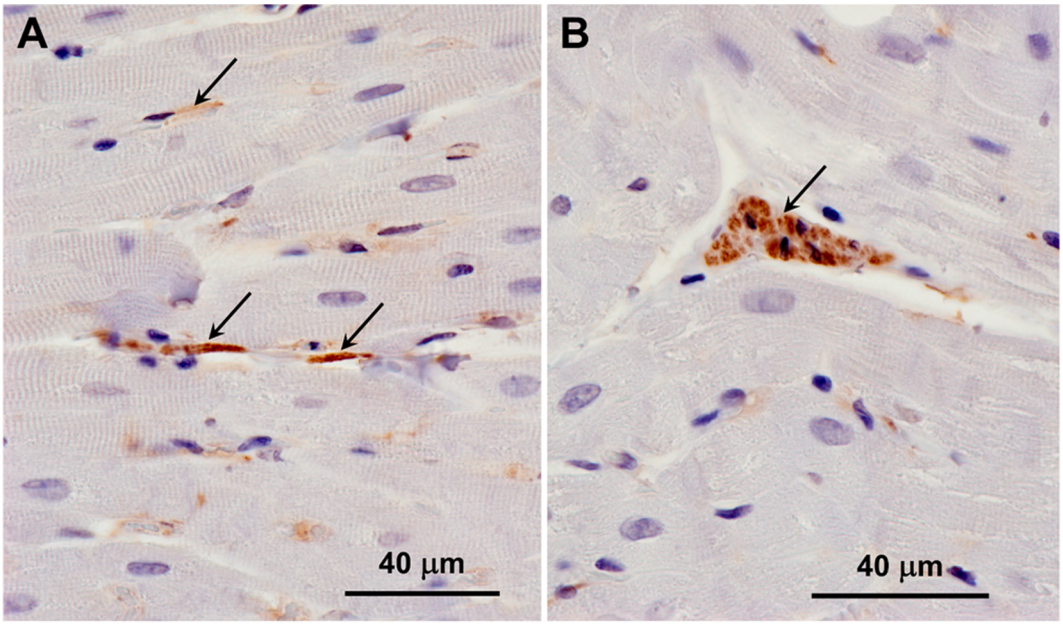

Fig. 20. Sections of the cardiac ventricular wall muscle from an unaffected Australian Shepherd in sections cut with muscle fibers mainly oriented longitudinally (A) or in cross-section (B). Sections were immunostained with an anti-CNPase antibody. Immunolabeling (arrows) was present in cells interposed between the muscle fibers.

and B may have resulted from lysosomal dysfunction secondary to impaired endosomal sorting of critical lysosomal components. In addition, if newly synthesized hydrolases normally destined for the lysosomes are instead transported to the cell surface or the extracellular space, it could explain the apparent progressive breakdown of the extrafascicular matrix in the optic nerves from the affected dogs (Vizovisek et al., 2019).

The phenotypic features of the disorders resulting from CNPase deficiencies indicate that these diseases should be considered for classification as a novel form of neuronal ceroid lipofuscinosis (NCL). The identification of autofluorescent lysosomal storage bodies in cases of hereditary progressive neurodegenerative disease has almost always led to a diagnosis of NCL, although there have been a few exceptions (Kowalewski et al., 2012; Lowden et al., 1981; Oldfors and Sourander, 1981; Wisniewski et al., 1985; Damme et al., 2011; Kolicheski et al., 2017). In many of the established forms of NCL, the subunit c protein of mitochondrial ATP synthase has been found to be sequestered in the storage bodies that accumulate in these diseases (Rowan and Lake, 1995; Katz et al., 1995; Hosain et al., 1995; Vesa and Peltonen, 2002; Cao et al., 2011; Pastores and Maegawa, 2013). The presence of this protein in the storage bodies in the affected Dalmatians supports the classification of the CNP-deficiency disease as a form of NCL since this protein does not appear to accumulate in other lysosomal storage diseases (Kominami et al., 1992). The mechanisms underlying the selective accumulation of this protein in the NCLs remain to be determined. To date, 13 genetically distinct forms of human NCL have been recognized, with each resulting from deleterious variants in a different gene (Butz et al., 2020). The different subtypes of NCL have been designated as

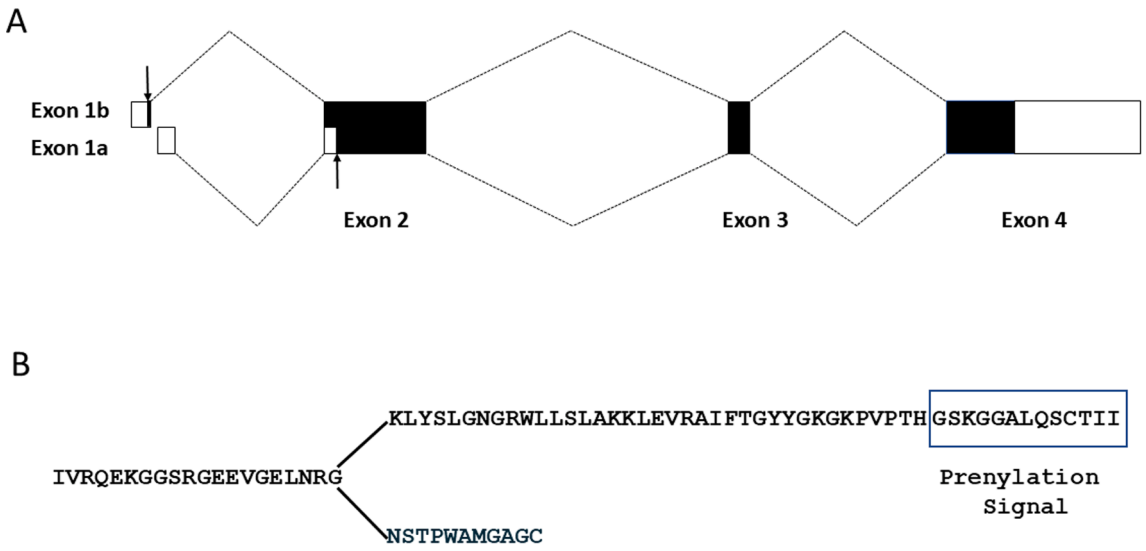

Fig. 21. CNPase isoforms and variant. (A) The two major CNPase isoforms result from utilization of alternative transcription initiation sites. The codon for the translation initiator methionine for the longer isoform is at the 3′ end of exon 1b. The translation initiator methionine for the shorter isoform is the twentieth codon in exon 2. Top dotted lines show the splicing pattern for the longer isoform; bottom dotted lines show the splicing pattern for the shorter isoform. Solid rectangles represent coding regions, open rectangles represent untranslated regions. Arrows show the positions of the initiator methionines. (B) The predicted codons for the C-terminal amino acid sequences encoded by the wildtype (upper) and variant (lower) canine *CNP* alleles. A reading-frame shift causes the predicted codons for the 51C-terminal amino acids including the 13 amino acid prenylation signal of the wildtype allele to be replaced by codons for 11 unrelated amino acids in the variant allele.

CLN1 to CLN8 and CLN10 to CLN14. The CLN9 designation was assigned in error and has been retired (Haddad et al., 2012). The identification of widespread and extensive accumulation of autofluorescent storage bodies in neurons from the brains of two human siblings with infantile hypotonia with psychomotor retardation and characteristic facies-3 (IHPRF3; OMIM: 616900) due to a homozygous nonsense mutation in *TBCK* has led to the proposal that IHPRF3 be classified as an NCL with the designation of CLN15 (Beck-Wodl et al., 2018). As with the storage granules from the Dalmatians A and B, many of the storage granules from the IHPRF3 patients contained lipid droplets. We propose that based on our findings, searches should be undertaken for potentially causal *CNP* variants in archived DNA from patients with progressive neurological diseases of unknown etiology and for autofluorescent storage bodies in tissues from future cases of human *CNP* deficiencies. This may lead to classification of the disorder resulting from *CNP* deficiency as a novel form of human NCL.

CRediT authorship contribution statement

Garrett Bullock: Methodology, Data curation, Writing – review & editing. **Gary S. Johnson:** Conceptualization, Writing – original draft, Writing – review & editing. **Tendai Mhlanga-Mutangadura:** Methodology. **Scott C. Petesch:** Writing – review & editing. **Samantha Thompson:** Writing – review & editing. **Sandra Goebbels:** Methodology, Investigation, Writing – review & editing. **Martin L. Katz:** Conceptualization, Writing – original draft, Methodology, Visualization, Investigation, Writing – review & editing.

Declaration of Competing Interest

The authors declare that they have no known competing financial interests or personal relationships that could have appeared to influence the work reported in this paper.

Acknowledgements

Our thanks to the dog owners who provided phenotypic information and tissue and DNA samples from their dogs. Our thanks to Dr. Lixing Reneker for providing us with some of the mouse tissue samples. Technical and logistical assistance provided by Liz Hansen and Cheryl Jensen played important roles in these studies. Funding for this work was provided by the American Kennel Club Canine Health Foundation Grant No. 02604 and the Patton Trust/BioNexus KC.

Appendix A. Supplementary data

Supplementary data to this article can be found online at https://doi.org/10.1016/j.gene.2022.146513.

References

Platt, F.M., d'Azzo, A., Davidson, B.L., Neufeld, E.F., Tifft, C.J., 2018. Lysosomal storage diseases. Nat Rev Dis Primers 4, 27.
Wilson, P.J., Morris, C.P., Anson, D.S., Occhiodoro, T., Bielicki, J., Clements, P.R., Hopwood, J.J., 1990. Hunter syndrome: isolation of an iduronate-2-sulfatase cDNA clone and analysis of patient DNA. Proc Natl Acad Sci U S A 87, 8531–8535.
Dworzak, F., Casazza, F., Mora, M., De Maria, R., Gronda, E., Baroldi, G., Rimoldi, M., Morandi, L., Cornelio, F., 1994. Lysosomal glycogen storage with normal acid maltase: a familial study with successful heart transplant. Neuromuscul Disord 4, 243–247.
R.Y. Wang, O.A. Bodamer, M.S. Watson, W.R. Wilcox, A.W.G.o.D.C.o.L.S. Diseases, Lysosomal storage diseases: diagnostic confirmation and management of presymptomatic individuals. Genet Med 13 (2011) 457-484.
Naseri, N., Sharma, M., Velinov, M., 2021. Autosomal dominant neuronal ceroid lipofuscinosis: Clinical features and molecular basis. Clin Genet 99, 111–118.
Beck-Wodl, S., Harzer, K., Sturm, M., Buchert, R., Ries, O., Mennel, H.D., Latta, E., Pagenstecher, A., Keber, U., 2018. Homozygous TBC1 domain-containing kinase (TBCK) mutation causes a novel lysosomal storage disease - a new type of neuronal ceroid lipofuscinosis (CLN15)? Acta Neuropathol Commun 6, 145.
Kowalewski, B., Lange, H., Galle, S., Dierks, T., Lubke, T., Damme, M., 2021. Decoding the consecutive lysosomal degradation of 3-O-sulfate containing heparan sulfate by Arylsulfatase G (ARSG). Biochem J 478, 3221–3237.
Gupta, P., Soyombo, A.A., Shelton, J.M., Wilkofsky, I.G., Wisniewski, K.E., Richardson, J. A., Hofmann, S.L., 2003. Disruption of PPT2 in mice causes an unusual lysosomal storage disorder with neurovisceral features. Proc Natl Acad Sci U S A 100, 12325–12330.
Poet, M., Kornak, U., Schweizer, M., Zdebik, A.A., Scheel, O., Hoelter, S., Wurst, W., Schmitt, A., Fuhrmann, J.C., Planells-Cases, R., Mole, S.E., Hubner, C.A., Jentsch, T. J., 2006. Lysosomal storage disease upon disruption of the neuronal chloride transport protein ClC-6. Proc Natl Acad Sci U S A 103, 13854–13859.
Stypmann, J., Gläser, K., Roth, W., Tobin, D.J., Petermann, I., Matthias, R., Mönnig, G., Haverkamp, W., Breithardt, G., Schmahl, W., Peters, C., Reinheckel, T., 2002. Dilated cardiomyopathy in mice deficient for the lysosomal cysteine peptidase cathepsin L. Proc Natl Acad Sci U S A 99 (9), 6234–6239.

Trabszo, C., Ramms, B., Chopra, P., Lullmann-Rauch, R., Stroobants, S., Spross, J., Jeschke, A., Schinke, T., Boons, G.J., Esko, J.D., Lubke, T., Dierks, T., 2020. Arylsulfatase K inactivation causes mucopolysaccharidosis due to deficient glucuronate desulfation of heparan and chondroitin sulfate. Biochem J 477, 3433–3451.

Yanagawa, M., Tsukuba, T., Nishioku, T., Okamoto, Y., Okamoto, K., Takii, R., Terada, Y., Nakayama, K.I., Kadowaki, T., Yamamoto, K., 2007. Cathepsin E deficiency induces a novel form of lysosomal storage disorder showing the accumulation of lysosomal membrane sialoglycoproteins and the elevation of lysosomal pH in macrophages. J Biol Chem 282, 1851–1862.

Abitbol, M., Thibaud, J.L., Olby, N.J., Hitte, C., Puech, J.P., Maurer, M., Pilot-Storck, F., Hedan, B., Dreano, S., Brahimi, S., Delattre, D., Andre, C., Gray, F., Delisle, F., Caillaud, C., Bernex, F., Panthier, J.J., Aubin-Houzelstein, G., Blot, S., Tiret, L., 2010. A canine Arylsulfatase G (ARSG) mutation leading to a sulfatase deficiency is associated with neuronal ceroid lipofuscinosis. Proc Natl Acad Sci U S A 107, 14775–14780.

Ahmed, Z., Sheng, H., Xu, Y.F., Lin, W.L., Innes, A.E., Gass, J., Yu, X., Wuertzer, C.A., Hou, H., Chiba, S., Yamanouchi, K., Leissring, M., Petrucelli, L., Nishihara, M., Hutton, M.L., McGowan, E., Dickson, D.W., Lewis, J., 2010. Accelerated lipofuscinosis and ubiquitination in granulin knockout mice suggest a role for progranulin in successful aging. Am J Pathol 177, 311–324.

Awano, T., Katz, M.L., O'Brien, D.P., Taylor, J.F., Evans, J., Khan, S., Sohar, I., Lobel, P., Johnson, G.S., 2006. A mutation in the cathepsin D gene (CTSD) in American Bulldogs with neuronal ceroid lipofuscinosis. Mol Genet Metab 87, 341–348.

Cooper, A., Hatton, C., Thornley, M., Sardharwalla, I.B., 1988. Human beta-mannosidase deficiency: biochemical findings in plasma, fibroblasts, white cells and urine. J Inherit Metab Dis 11, 17–29.

Farias, F.H., Zeng, R., Johnson, G.S., Wininger, F.A., Taylor, J.F., Schnabel, R.D., McKay, S.D., Sanders, D.N., Lohi, H., Seppala, E.H., Wade, C.M., Lindblad-Toh, K., O'Brien, D.P., Katz, M.L., 2011. A truncating mutation in ATP13A2 is responsible for adult-onset neuronal ceroid lipofuscinosis in Tibetan terriers. Neurobiol Dis 42, 468–474.

Jones, M.Z., Dawson, G., 1981. Caprine beta-mannosidosis. Inherited deficiency of beta-D-mannosidase. J Biol Chem 256, 5185–5188.

Kowalewski, B., Lamanna, W.C., Lawrence, R., Damme, M., Stroobants, S., Padva, M., Kalus, I., Frese, M.A., Lubke, T., Lullmann-Rauch, R., D'Hooge, R., Esko, J.D., Dierks, T., 2012. Arylsulfatase G inactivation causes loss of heparan sulfate 3-O-sulfatase activity and mucopolysaccharidosis in mice. Proc Natl Acad Sci U S A 109, 10310–10315.

Tang, C.H., Lee, J.W., Galvez, M.G., Robillard, L., Mole, S.E., Chapman, H.A., 2006. Murine cathepsin F deficiency causes neuronal lipofuscinosis and late-onset neurological disease. Mol Cell Biol 26, 2309–2316.

Tyynela, J., Sohar, I., Sleat, D.E., Gin, R.M., Donnelly, R.J., Baumann, M., Haltia, M., Lobel, P., 2000. A mutation in the ovine cathepsin D gene causes a congenital lysosomal storage disease with profound neurodegeneration. EMBO J 19, 2786–2792.

Siintola, E., Partanen, S., Stromme, P., Haapanen, A., Haltia, M., Maehlen, J., Lehesjoki, A.E., Tyynela, J., 2006. Cathepsin D deficiency underlies congenital human neuronal ceroid-lipofuscinosis. Brain 129, 1438–1445.

Smith, K.R., Dahl, H.H., Canafoglia, L., Andermann, E., Damiano, J., Morbin, M., Bruni, A.C., Giaccone, G., Cossette, P., Saftig, P., Grotzinger, J., Schwake, M., Andermann, F., Staropoli, J.F., Sims, K.B., Mole, S.E., Franceschetti, S., Alexander, N. A., Cooper, J.D., Chapman, H.A., Carpenter, S., Berkovic, S.F., Bahlo, M., 2013. Cathepsin F mutations cause Type B Kufs disease, an adult-onset neuronal ceroid lipofuscinosis. Hum Mol Genet 22, 1417–1423.

Smith, K.R., Damiano, J., Franceschetti, S., Carpenter, S., Canafoglia, L., Morbin, M., Rossi, G., Pareyson, D., Mole, S.E., Staropoli, J.F., Sims, K.B., Lewis, J., Lin, W.L., Dickson, D.W., Dahl, H.H., Bahlo, M., Berkovic, S.F., 2012. Strikingly different clinicopathological phenotypes determined by progranulin-mutation dosage. Am J Hum Genet 90, 1102–1107.

Wenger, D.A., Sujansky, E., Fennessey, P.V., Thompson, J.N., 1986. Human beta-mannosidase deficiency. N Engl J Med 315, 1201–1205.

Al-Abdi, L., Al Murshedi, F., Elmanzalawy, A., Al Habsi, A., Helaby, R., Ganesh, A., Ibrahim, N., Patel, N., Alkuraya, F.S., 2020. CNP deficiency causes severe hypomyelinating leukodystrophy in humans. Hum Genet 139, 615–622.

C. Lappe-Siefke, S. Goebbels, M. Gravel, E. Nicksch, J. Lee, P.E. Braun, I.R. Griffiths, K.A. Nave, Disruption of Cnp1 uncouples oligodendroglial functions in axonal support and myelination. 1 (2003) 366-374.

Whiting, R.E.H., Pearce, J.W., Vansteenkiste, D.P., Bibi, K., Lim, S., Robinson Kick, G., Castaner, L.J., Sinclair, J., Chandra, S., Nguyen, A., O'Neill, C.A., Katz, M.L., 2020. Intravitreal enzyme replacement preserves retinal structure and function in canine CLN2 neuronal ceroid lipofuscinosis. Experimental Eye Research 197, 108130. https://doi.org/10.1016/j.exer.2020.108130.

Katz, M.L., Parker, K.R., Handelman, G.J., Bramel, T.L., Dratz, E.A., 1982. Effects of antioxidant nutrient deficiency on the retina and retinal pigment epithelium of albino rats: a light and electron microscopic study. Experimental Eye Research 34, 339–369.

Villani, N.A., Bullock, G., Michaels, J.R., Yamato, O., O'Brien, D.P., Mhlanga-Mutangadura, T., Johnson, G.S., Katz, M.L., 2019. A mixed breed dog with neuronal ceroid lipofuscinosis is homozygous for a CLN5 nonsense mutation previously identified in Border Collies and Australian Cattle Dogs. Mol Genet Metab 127, 107–115.

Morgan, B.R., Coates, J.R., Johnson, G.C., Bujnak, A.C., Katz, M.L., 2013. Characterization of intercostal muscle pathology in canine degenerative myelopathy: a disease model for amyotrophic lateral sclerosis. J Neurosci Res 91, 1639–1650.

Katz, M.L., Khan, S., Awano, T., Shahid, S.A., Siakotos, A.N., Johnson, G.S., 2005. A mutation in the CLN8 gene in English Setter dogs with neuronal ceroid-lipofuscinosis. Biochem Biophys Res Commun 327, 541–547.

Whiting, R.E., Narfstrom, K., Yao, G., Pearce, J.W., Coates, J.R., Castaner, L.J., Jensen, C. A., Dougherty, B.N., Vuillemenot, B.R., Kennedy, D., O'Neill, C.A., Katz, M.L., 2014. Enzyme replacement therapy delays pupillary light reflex deficits in a canine model of late infantile neuronal ceroid lipofuscinosis. Experimental Eye Research 125, 164–172.

Evans, A., Jeffery, G., 1992. The Fascicular Organization of the Cat Optic-Nerve. Exp Brain Res 91, 79–84.

Gherghiceanu, M., Popescu, L.M., 2012. Cardiac telocytes - their junctions and functional implications. Cell Tissue Res 348, 265–279.

Kostin, S., 2016. Cardiac telocytes in normal and diseased hearts. Semin Cell Dev Biol 55, 22–30.

Rowan, S.A., Lake, B.D., 1995. Tissue and cellular distribution of subunit c of ATP synthase in Batten disease (neuronal ceroid-lipofuscinosis). Am J Med Genet 57, 172–176.

Katz, M.L., Gao, C.L., Tompkins, J.A., Bronson, R.T., Chin, D.T., 1995. Mitochondrial ATP synthase subunit c stored in hereditary ceroid-lipofuscinosis contains trimethyl-lysine. Biochem J 310 (Pt 3), 887–892.

Hosain, S., Kaufmann, W.E., Negrin, G., Watkins, P.A., Siakotos, A.N., Palmer, D.N., Naidu, S., 1995. Diagnoses of neuronal ceroid-lipofuscinosis by immunochemical methods. Am J Med Genet 57, 239–245.

Vesa, J., Peltonen, L., 2002. Mutated genes in juvenile and variant late infantile neuronal ceroid lipofuscinoses encode lysosomal proteins. Curr Mol Med 2, 439–444.

Cao, Y.i., Staropoli, J.F., Biswas, S., Espinola, J.A., MacDonald, M.E., Lee, J.-M., Cotman, S.L., Sugihara, I., 2011. Distinct early molecular responses to mutations causing vLINCL and JNCL presage ATP synthase subunit C accumulation in cerebellar cells. PLoS ONE 6 (2), e17118.

Edgar, J.M., McLaughlin, M., Werner, H.B., McCulloch, M.C., Barrie, J.A., Brown, A., Faichney, A.B., Snaidero, N., Nave, K.A., Griffiths, I.R., 2009. Early ultrastructural defects of axons and axon-glia junctions in mice lacking expression of Cnp1. Glia 57, 1815–1824.

Rasband, M.N., Tayler, J., Kaga, Y., Yang, Y., Lappe-Siefke, C., Nave, K.A., Bansal, R., 2005. CNP is required for maintenance of axon-glia interactions at nodes of Ranvier in the CNS. Glia 50, 86–90.

Hagemeyer, N., Goebbels, S., Papiol, S., Kastner, A., Hofer, S., Begemann, M., Gerwig, U. C., Boretius, S., Wieser, G.L., Ronnenberg, A., Gurvich, A., Heckers, S.H., Frahm, J., Nave, K.A., Ehrenreich, H., 2012. A myelin gene causative of a catatonia-depression syndrome upon aging. EMBO Mol Med 4, 528–539.

Peirce, T.R., Bray, N.J., Williams, N.M., Norton, N., Moskvina, V., Preece, A., Haroutunian, V., Buxbaum, J.D., Owen, M.J., O'Donovan, M.C., 2006. Convergent evidence for 2',3'-cyclic nucleotide 3'-phosphodiesterase as a possible susceptibility gene for schizophrenia. Arch Gen Psychiatry 63, 18–24.

Mitkus, S.N., Hyde, T.M., Vakkalanka, R., Kolachana, B., Weinberger, D.R., Kleinman, J. E., Lipska, B.K., 2008. Expression of oligodendrocyte-associated genes in dorsolateral prefrontal cortex of patients with schizophrenia. Schizophr Res 98, 129–138.

Iwamoto, K., Ueda, J., Bundo, M., Nakano, Y., Kato, T., 2008. Effect of a functional single nucleotide polymorphism in the 2',3'-cyclic nucleotide 3'-phosphodiesterase gene on the expression of oligodendrocyte-related genes in schizophrenia. Psychiatry Clin Neurosci 62, 103–108.

Tang, F., Qu, M., Wang, L., Ruan, Y., Lu, T., Zhang, H., Liu, Z., Yue, W., Zhang, D., 2007. Case-control association study of the 2',3'-cyclic nucleotide 3'-phosphodiesterase (CNP) gene and schizophrenia in the Han Chinese population. Neurosci Lett 416, 113–116.

Voineskos, A.N., de Luca, V., Bulgin, N.L., van Adrichem, Q., Shaikh, S., Lang, D.J., Honer, W.G., Kennedy, J.L., 2008. A family-based association study of the myelin-associated glycoprotein and 2',3'-cyclic nucleotide 3'-phosphodiesterase genes with schizophrenia. Psychiatr Genet 18, 143–146.

Usui, H., Takahashi, N., Saito, S., Ishihara, R., Aoyama, N., Ikeda, M., Suzuki, T., Kitajima, T., Yamanouchi, Y., Kinoshita, Y., Yoshida, K., Iwata, N., Inada, T., Ozaki, N., 2006. The 2',3'-cyclic nucleotide 3'-phosphodiesterase and oligodendrocyte lineage transcription factor 2 genes do not appear to be associated with schizophrenia in the Japanese population. Schizophr Res 88, 245–250.

Che, R., Tang, W., Zhang, J., Wei, Z., Zhang, Z., Huang, K., Zhao, X., Gao, J., Zhou, G., Huang, P., He, L., Shi, Y., 2009. No relationship between 2',3'-cyclic nucleotide 3'-phosphodiesterase and schizophrenia in the Chinese Han population: an expression study and meta-analysis. BMC Med Genet 10, 31.

Cannon, D.M., Walshe, M., Dempster, E., Collier, D.A., Marshall, N., Bramon, E., Murray, R.M., McDonald, C., 2012. The association of white matter volume in psychotic disorders with genotypic variation in NRG1, MOG and CNP: a voxel-based analysis in affected individuals and their unaffected relatives. Transl Psychiatry 2, e167.

Janova, H., Arinrad, S., Balmuth, E., Mitjans, M., Hertel, J., Habes, M., Bittner, R.A., Pan, H., Goebbels, S., Begemann, M., Gerwig, U.C., Langner, S., Werner, H.B., Kittel-Schneider, S., Homuth, G., Davatzikos, C., Volzke, H., West, B.L., Reif, A., Grabe, H. J., Boretius, S., Ehrenreich, H., Nave, K.A., 2018. Microglia ablation alleviates myelin-associated catatonic signs in mice. J Clin Invest 128, 734–745.

Kurihara, T., Monoh, K., Sakimura, K., Takahashi, Y., 1990. Alternative splicing of mouse brain 2',3'-cyclic-nucleotide 3'-phosphodiesterase mRNA. Biochem Biophys Res Commun 170 (3), 1074–1081.

Lee, J., O'Neill, R.C., Park, M.W., Gravel, M., Braun, P.E., 2006. Mitochondrial localization of CNP2 is regulated by phosphorylation of the N-terminal targeting signal by PKC: implications of a mitochondrial function for CNP2 in glial and non-glial cells. Mol Cell Neurosci 31, 446–462.

Bifulco, M., Laezza, C., Stingo, S., Wolff, J., 2002. 2',3'-Cyclic nucleotide 3'-phosphodiesterase: a membrane-bound, microtubule-associated protein and membrane anchor for tubulin. Proc Natl Acad Sci U S A 99, 1807–1812.

Esposito, C., Scrima, M., Carotenuto, A., Tedeschi, A., Rovero, P., D'Errico, G., Malfitano, A.M., Bifulco, M., D'Ursi, A.M., 2008. Structures and micelle locations of the nonlipidated and lipidated C-terminal membrane anchor of 2',3'-cyclic nucleotide-3'-phosphodiesterase. Biochemistry 47, 308–319.

Braun, P.E., De Angelis, D., Shtybel, W.W., Bernier, L., 1991. Isoprenoid modification permits 2',3'-cyclic nucleotide 3'-phosphodiesterase to bind to membranes. J Neurosci Res 30, 540–544.

Verrier, J.D., Jackson, T.C., Gillespie, D.G., Janesko-Feldman, K., Bansal, R., Goebbels, S., Nave, K.A., Kochanek, P.M., Jackson, E.K., 2013. Role of CNPase in the oligodendrocytic extracellular 2',3'-cAMP-adenosine pathway. Glia 61, 1595–1606.

Azarashvili, T., Krestinina, O., Galvita, A., Grachev, D., Baburina, Y., Stricker, R., Evtodienko, Y., Reiser, G., 2009. Ca2+-dependent permeability transition regulation in rat brain mitochondria by 2',3'-cyclic nucleotides and 2',3'-cyclic nucleotide 3'-phosphodiesterase. Am J Physiol Cell Physiol 296 (6), C1428–C1439.

Olga, K., Yulia, B., Vassilios, P., 2020. The Functions of Mitochondrial 2',3'-Cyclic Nucleotide-3'-Phosphodiesterase and Prospects for Its Future. Int J Mol Sci 21 (9), 3217. https://doi.org/10.3390/ijms21093217.

Laezza, C., Wolff, J., Bifulco, M., 1997. Identification of a 48-kDa prenylated protein that associates with microtubules as 2',3'-cyclic nucleotide 3'-phosphodiesterase in FRTL-5 cells. FEBS Lett 413, 260–264.

De Angelis, D.A., Braun, P.E., 1996. 2',3'-Cyclic nucleotide 3'-phosphodiesterase binds to actin-based cytoskeletal elements in an isoprenylation-independent manner. J Neurochem 67, 943–951.

Snaidero, N., Velte, C., Myllykoski, M., Raasakka, A., Ignatev, A., Werner, H.B., Erwig, M. S., Mobius, W., Kursula, P., Nave, K.A., Simons, M., 2017. Antagonistic Functions of MBP and CNP Establish Cytosolic Channels in CNS Myelin. Cell Rep 18, 314–323.

Lee, J., Gravel, M., Zhang, R., Thibault, P., Braun, P.E., 2005. Process outgrowth in oligodendrocytes is mediated by CNP, a novel microtubule assembly myelin protein. J Cell Biol 170, 661–673.

Gravel, M., Robert, F., Kottis, V., Gallouzi, I.E., Pelletier, J., Braun, P.E., 2009. 2',3'-Cyclic nucleotide 3'-phosphodiesterase: a novel RNA-binding protein that inhibits protein synthesis. J Neurosci Res 87, 1069–1079.

Anitei, M., Hoflack, B., 2011. Bridging membrane and cytoskeleton dynamics in the secretory and endocytic pathways. Nat Cell Biol 14, 11–19.

Vizovisek, M., Fonovic, M., Turk, B., 2019. Cysteine cathepsins in extracellular matrix remodeling: Extracellular matrix degradation and beyond. Matrix Biol 75–76, 141–159.

Lowden, J.A., Callahan, J.W., Gravel, R.A., Skomorowski, M.A., Becker, L., Groves, J., 1981. Type 2 GM1 gangliosidosis with long survival and neuronal ceroid lipofuscinosis. Neurology 31, 719–724.

Oldfors, A., Sourander, P., 1981. Storage of lipofuscin in neurons in mucopolysaccharidosis. Report on a case of Sanfilippo's syndrome with histochemical and electron-microscopic findings. Acta Neuropathol 54, 287–292.

Wisniewski, K., Rudelli, R., Laure-Kamionowska, M., Sklower, S., Houck Jr., G.E., Kieras, F., Ramos, P., Wisniewski, H.M., Braak, H., 1985. Sanfilippo disease, type A with some features of ceroid lipofuscinosis. Neuropediatrics 16, 98–105.

Damme, M., Stroobants, S., Walkley, S.U., Lullmann-Rauch, R., D'Hooge, R., Fogh, J., Saftig, P., Lubke, T., Blanz, J., 2011. Cerebellar alterations and gait defects as therapeutic outcome measures for enzyme replacement therapy in alpha-mannosidosis. J Neuropathol Exp Neurol 70, 83–94.

Kolicheski, A., Johnson, G.S., Villani, N.A., O'Brien, D.P., Mhlanga-Mutangadura, T., Wenger, D.A., Mikoloski, K., Eagleson, J.S., Taylor, J.F., Schnabel, R.D., Katz, M.L., 2017. GM2 Gangliosidosis in Shiba Inu Dogs with an In-Frame Deletion in HEXB. J Vet Intern Med 31, 1520–1526.

Pastores, G.M., Maegawa, G.H.B., 2013. Clinical Neurogenetics: Neuropathic Lysosomal Storage Disorders. Neurologic Clinics 31, 1051–1071.

Kominami, E., Ezaki, J., Muno, D., Ishido, K., Ueno, T., Wolfe, L.S., 1992. Specific storage of subunit c of mitochondrial ATP synthase in lysosomes of neuronal ceroid lipofuscinosis (Batten's disease). J Biochem 111, 278–282.

Butz, E.S., Chandrachud, U., Mole, S.E., Cotman, S.L., 2020. Moving towards a new era of genomics in the neuronal ceroid lipofuscinoses. Biochimica et Biophysica Acta (BBA) - Molecular Basis of Disease 1866 (9), 165571. https://doi.org/10.1016/j.bbadis.2019.165571.

Haddad, S.E., Khoury, M., Daoud, M., Kantar, R., Harati, H., Mousallem, T., Alzate, O., Meyer, B., Boustany, R.M., 2012. CLN5 and CLN8 protein association with ceramide synthase: biochemical and proteomic approaches. Electrophoresis 33, 3798–3809.